1974

Surface electromagnetic waves with damping I. Isotropic Media II. Anisotropic Media

Gary Shannon Kovener

Department: Physics

SURFACE ELECTROMAGNETIC WAVES WITH DAMPING

I. ISOTROPIC MEDIA

II. ANISOTROPIC MEDIA

by

GARY SHANNON KOVENER, 1946-

A DISSERTATION

Presented to the Faculty of the Graduate School of the

UNIVERSITY OF MISSOURI-ROLLA

In Partial Fulfillment of the Requirements for the Degree

DOCTOR OF PHILOSOPHY

in

PHYSICS

1974

Ralph W. Alexander Jr
Advisor

L. F. Severston

R J Bell

Gary J. Long

J. L. Peacher

PUBLICATION THESIS OPTION

This thesis has been prepared in the style utilized by the Physical Review. Part I: Isotropic Media and Part II: Anisotropic Media will be presented separately for publication in that journal. In addition, the following publications are submitted in partial fulfillment of the Ph.D. degree and may be found elsewhere:

"Surface Excitations in Absorbing Media", R. J. Bell, R. W. Alexander, Jr., W. F. Parks, and G. Kovener, Optics Comm. 8, 147 (1973).

"Dispersion Curves for Surface Electromagnetic Waves with Damping", R. W. Alexander, G. S. Kovener, and R. J. Bell, Phys. Rev. Lett. 32, 154 (1974).

ACKNOWLEDGEMENTS

The list of those persons who have contributed to this work is a long list. The contribution of some individuals was financial, the contribution of others was intellectual and the contribution of a few could be charitably described as negligible.

I therefore will limit the acknowledgements to those persons with whom I had a formal arrangement. The inestimable help of my advisor, Dr. Ralph W. Alexander, Jr. and the aid of Dr. Robert J. Bell are greatly appreciated.

The contribution of my wife, Sharon, to this work cannot be categorized; rather, it was that nebulous aid given to all successful graduate students by their spouse.

TABLE OF CONTENTS

Table of Contents (continued) Page

ATR REFLECTIVITY STUDY OF SURFACE ELECTROMAGNETIC WAVES WITH DAMPING†

by

G. S. Kovener, R. W. Alexander, Jr.,
I. L. Tyler, and R. J. Bell

Graduate Center for Materials Research
and Physics Department
University of Missouri-Rolla
Rolla, Missouri 65401

ABSTRACT

Surface electromagnetic wave (SEW) dispersion curves are usually calculated using a simple equation derived from Maxwell's equations and boundary conditions. When complex dielectric functions are used for the two media, the component of the propagation vector along the surface k_x becomes infinite as the frequency ω approaches the surface polariton frequency ω_s if ω is considered complex and k_x real. On the other hand, if k_x is considered complex and ω real, the dispersion curves bend back toward smaller k_x as ω approaches ω_s. We have previously demonstrated that both types of dispersion curves can be obtained from attenuated total reflection measurements of silver. We now extend this result to other materials and show that dispersion curves alone present an inadequate summary of the data.

I. INTRODUCTION

Dispersion curves for elementary excitations are usually treated in the absence of damping and inclusion of damping considerably complicates the situation.[1-3] This has been pointed out for bulk excitations by Barker and Loudon.[4] In this paper we shall restrict ourselves to surface electromagnetic waves (SEW) on isotropic media and postpone a discussion of anisotropic media.[5] We show that there is an ambiguity in what is meant by the dispersion curves when damping is present and further that care must be exercised in relating the minima in reflectivity observed using ATR techniques to the dispersion curves. Following a general discussion, we will consider three classes of SEW: surface plasmons, surface phonons and coupled surface plasmon-surface phonons. The effects of finite beam divergence will also be considered and shown to be important in some cases.

II. DISPERSION CURVES WITH DAMPING

To simplify our discussion, we shall consider SEW on an infinite half-space, $z<0$, with the $z>0$ half-space being vacuum. Then the dispersion curves for SEW are the solutions to [1,6]

$$k_x = \frac{\omega}{c}\left\{\frac{\varepsilon(\omega)}{\varepsilon(\omega)+1}\right\}^{1/2} \qquad (1)$$

where $\varepsilon(\omega) = \varepsilon_1(\omega) + i\varepsilon_2(\omega)$ is the dielectric function of the medium and k_x is the component of the propagation vector along the surface. Usually $\varepsilon_2(\omega)$ is considered to vanish, and then k_x is purely real for those frequencies for which SEW exist, i.e., those frequencies for which $\varepsilon_1(\omega) < -1$. In the absence of damping, $k_x \to \infty$ at the surface wave frequency ω_s where $\varepsilon_1(\omega_s) = -1$.

In the presence of damping, $\varepsilon_2(\omega) \neq 0$, Eq. (1) becomes complex and if ω is chosen to be real, then k_x is complex. The real part of k_x describes the propagation wavevector and the imaginary part of k_x describes the spatial damping in a manner frequently encountered in optics.[7] The real part k_{1x} of k_x is used to plot the dispersion curve. In this case, however, the dispersion curves bend back toward smaller k_{1x} as ω approaches ω_s, rather than k_{1x} becoming infinite at this frequency.[6] This difference in behavior is illustrated in Fig. 1 where the dielectric function for silver has been used.[8] The dashed line is for $\varepsilon_2 = 0$ and the solid line for $\varepsilon_2 \neq 0$. For the moment ignore the curves above ω_s.

Because the propagation vector, k, has become complex, the usual condition for the existence of surface waves can no longer be used. This condition requires k_z, the z-component of k, to be purely imaginary so the fields decay exponentially away from the surface in both the + and - z directions (which requires $\varepsilon(\omega) < -1$). With $\varepsilon(\omega)$

complex, k_z is complex so this evanescent wave condition is no longer useful. Instead we shall replace it with the condition that $\varepsilon_1(\omega) < -1$.

Another method of finding the dispersion curve for $\varepsilon(\omega)$ complex is to keep k real and let ω be complex.[9,10] The equations to be solved are complicated and cannot in general be solved analytically. The solution has been found numerically by Gammon and Palik[9] who find the resulting dispersion curve to be very close to that obtained using real $\varepsilon(\omega)$. That is, no bend back occurs, and k_x becomes large as ω approaches ω_s. Thus, when damping is included, we can obtain two dispersion curves, depending upon whether we keep ω real and k complex, or treat k real and ω complex. This is an indication that a plot of ω vs k cannot represent all the information present in $\varepsilon(\omega)$ if $\varepsilon(\omega)$ is complex.

A similar problem for bulk polaritons within the context of Raman scattering[4,11-14] has been discussed in the literature. Several authors[11-14] have used a temporal damping (ω complex) treatment for bulk polaritons which have the usual dispersion relation

$$k = (\omega/c)\sqrt{\varepsilon}. \qquad (2)$$

The real ω roots of the polynomial do not exhibit bend back as k_x increases, but the roots asymptotically approach a limiting frequency. However, Giallorenzi[14] points out

that the solution does not differ substantially from that obtained by taking only the real part of $\varepsilon(\omega)$, just as for SEW.

Puthoff, et al.[15] have made the calculation keeping ω real and found the dispersion curves also bend back in a manner similar to that found for SEW dispersion curves with k_x complex.

Another way to understand this difficulty with the dispersion curves is to consider it as an attempt to describe the normal modes of a system that has damping. If one considers the excitation as a wave propagating along a surface, then spatial damping (complex k_x) is appropriate. Conversely viewed as an excitation of a normal mode that decays in time, temporal damping (complex ω) is required.

The way to avoid these difficulties is to consider the quantities measured in the experiment. For ATR experiments this quantity is the reflectivity as a function of ω and k_{1x}. In practice one measures the angle of incidence, θ, and relates this to k_{1x} by

$$k_{1x} = (\omega/c)\, n_p \sin\theta \qquad (3)$$

The results can be represented by a three-dimensional plot of the reflectivity versus both θ and ω. A typical calculated surface is shown in Fig. 2 for silver.

The real and imaginary parts of the dielectric

function were taken from Johnson and Christy.[8] The equations of Wolter[16] for the reflectivity of a multilayer media were used with the experimental geometry as shown in the inset. No correction was applied for losses at the hemicylinder entrance and exit faces. The refractive index of the CaF_2 hemicylinder was 1.434 and the film was 340 A thick. The range of ω was 3.0 to 4.25 eV, with the range of incident angles from 45° to 75°.

There are two valleys in this reflectance surface. The lower energy valley is due to surface plasmons while the other valley is due to a bulk plasmons ($\varepsilon_1(\omega)=0$).

In practice, experimentalists have chosen one of two methods to measure this reflectivity surface.[3,17-20] If the experiment is done by fixing the angle and scanning the frequency, the ATR spectra is a cross section line going from left to right. Alternatively if the frequency is fixed and the angle scanned, the ATR spectra is a cross section line going from bottom to top. Some representative cross sections are shown in Figs. 3a and 3b. The frequencies of successive cross section minima are converted to momenta using the ATR equation [Eq. (3)] and then plotted in Fig. 1. The dashed line is the result obtained for fixed angle cross sections and the solid line for fixed frequency cross sections. It is evident that the dashed curve approaches an asymptote while the solid line bends back. The crosses are the data

points of Arakawa, et al., and the slight discrepancy near 3.7 eV is due to sample differences between Johnson and Christy and Arakawa, et al.[20] In this region, the real part of $\varepsilon(\omega)$ approaches -1, and the ATR reflectivity minima are sensitive to small variations in $\varepsilon(\omega)$.

The reason for the bend back using fixed frequencies can be seen qualitatively by a careful examination of the reflectance surface. As one selects successive fixed energy cross sections the spectra obtained become more and more parallel to the axis of the SEW valley near 3.7 eV. When the energy is sufficiently large the spectra are no longer located in the minimum of this valley but climb the ridge between valleys. The curves of Fig. 3b clearly illustrate this anomalous behavior.

The solid curve also represents the solution of Eq. (1) for ω real and k_x complex with $\varepsilon(\omega)$ complex. The bend back is in agreement with the previous discussion. The dashed curve is the solution of Eq. (1) for $\mathrm{Im}(\varepsilon(\omega))\equiv 0$, and it approaches a frequency asymptote as expected. Thus our approach of three dimensional reflectance surfaces correctly predicts the experimental results and the results for both ω real, k_x complex and ω complex, k_x real. It also demonstrates the ambiguity in calling the ATR results the "dispersion curve".

III. APPLICATIONS

The reflectance surface is an ideal way of easily visualizing the influence of the gap spacing in those ATR measurements with an air gap between the sample and prism (Fig. 4). The gap spacing is an important factor in determining the features of the spectra since there are two fields exponentially decaying across the gap. One field due to the incident light has its maximum at the prism-gap interface. The other evanescent field is due to the SEW and has its maximum value at the gap-absorber interface. For small gaps the SEW may recouple back into the prism but the effect of gap spacing is also influenced by the value of ω and k_x. An expression for the optimum gap spacing has been derived by Otto[21] with some approximations but because the reflectance surface displays the response for a wide range of ω and θ, it is a more effective aid for looking at this gap dependence.

NaCl was chosen for this investigation since it has been examined experimentallly by Bryksin, et al.[22] In this case the NaCl sample was separated from the base of the prism by various air gap spacings. The calculations were done for frequencies from 150 cm^{-1} to 250 cm^{-1} and incident angles from 20° to 60° in the prism (silicon, $n_p = 3.418$). The reflectance surfaces were generated for several air gap spacings: 12 μm, 5 μm and 2 μm. The

NaCl dielectric function was calculated from the oscillator model and the parameters of Bryksin, et al.[22] (Table I). The phonon damping was not frequency dependent and was assumed a constant for each oscillator.

Two reflectance surfaces are presented here for comparison: Fig. 5 with a gap spacing of 5.0 μm and Fig. 6 with a gap of 12.0 μm. Although the surface of Fig. 5 is for a smaller gap, the overall reflectance minima are shallower and broader which is a general consequence of recoupling back into the prism. In addition, the "valley" of Fig. 5 clearly "turns" toward smaller frequencies as θ is decreased. Note the sharp rise in reflectivity of the SEW minima near the critical angle (17° for a silicon prism).

The dispersion curves resulting from the minima are shown in Fig. 7. (To compute these minima a smaller grid was used than that of Figs. 5 and 6.) The solid curves B and C are obtained from minima with frequency fixed; dashed curves B and C are obtained with incident angle fixed. Curve B is with a 5.0 μm gap and curve C with a 2.0 μm gap. The triangles correspond to a gap of 12.0 μm and for clarity are not connected with a smooth curve. The crosses are the experimental points obtained from Bryksin, et al.[22] The value of the gap spacing they used is not given, but we estimate from the reflectance spectra given in their article that $d \sim 10 - 11$ μm. The solid

line A is obtained from Eq. (1) with $\mathrm{Im}(\varepsilon(\omega))=0$ and the dashed line A using a complex $\varepsilon(\omega)$ and the real part of k_x.

The reflectance minima curve approaches the calculated dispersion curve Eq. (1) at small k only for large gap spacings. This is expected since the SEW will strongly couple to the prism via the evanescent field of the SEW at small gaps. Indefinitely large gaps cannot be used since the reflectivity minimum is substantially reduced at larger angles for large gaps as can be seen by comparing the reflectance surfaces of Fig. 5 and Fig. 6.[23] However, for all gap spacings, the fixed angle minima (dashed curves) approach the asymptote of Eq. (1) for sufficiently large k, but the experimental data appear to approach an asymptote of lower frequency, as noted by Bryksin, et al.[22] We attempted to improve the fit by considering a finite beam as discussed in the next section, but no appreciable change was noted in the reflectance minima curves.

It is therefore certain that the discrepancy in frequencies is not due to recoupling across the gap or finite beam divergence. Because the purpose of this paper is to demonstrate the reflectance surface technique we have not attempted different damping parameters or frequency dependent damping parameters in an attempt to reconcile the difference. The ability of the reflectance surfaces to easily represent all facets of the gap spacing is obvious.

The full width half-maximum (FWHM) of the ATR spectra is of interest because it is an indication of the damping of the SEW and thereby the absorbing material. We have found that a straightforward measurement of FWHM and its conversion to the material damping parameter does not include all the parameters which determine the FWHM. One can decide from an examination of the reflectance surface that the FWHM is also controlled by the gap spacing and the incident angle in a manner that is difficult to perceive with other analytical techniques. That is, the ATR cross sections measured do not cross the valleys at right angles, and this increases the observed width of the spectra. Once again, we will select an example to demonstrate this.

InSb has been studied extensively using the grating technique[24,25] and the ATR technique.[18,26] Although no appreciable difference is apparent between calculated and measured SEW dispersion curves, the ATR line width of the upper branch is larger by two to three times the width expected from the bulk electronic damping constant τ. We will include the finite beam divergence using an integrated spectra approach in an attempt to reduce this line width discrepancy.

The free carrier concentration in InSb produces strong plasmon-phonon coupling for electron concentrations on the order of 10^{17} cm^{-3}. In addition, the conduction

band is non-parabolic so the effective mass m* is a function of the concentration.[27] For a carrier concentration of 2.0×10^{17} cm^{-3} there are two frequency regions for SEW: $\omega < \omega_{TO}$ and $\omega_{TO} < \omega < \omega_p$. These two branches are readily visible on the 3-D surface of Fig. 8. The incident frequency is from 150 to 250 cm^{-1} and incident angles are from 18 to 38°. The ATR prism is silicon and gap is 19 μm. The InSb parameters used to calculate the dielectric function are given in Table II.

A fixed angle cross section for $\theta = 22°$ is detailed in Fig. 9. The crosses in Fig. 9 are the experimental data of Bryksin, et al.[26] for the lower branch (A) and the upper branch (B). The dashed line is the calculated ATR spectra with the electronic lifetime $\tau = 10$ cm^{-1}. A better fit is obtained with $\tau = 20$ cm^{-1} which is shown as the solid line. Similar changes of the oscillator damping Γ did not appreciably alter the lower branch fit.

One must be very careful in relating the FWHM of the ATR spectra to the damping of the SEW. The shape of the minima is determined by the ATR parameters of θ and gap spacing d as well as the material parameters. The influence of θ and d on the width is clearly apparent in the Figs. 5 and 6 for NaCl. Therefore, if one desires to measure the material damping using SEW, the experimental variables θ and d must be accurately measured and d should be uniform.

The finite divergence of the incident beam is considered by integrating at a fixed frequency over a range of incident angles centered about θ_0. The reflectivity is weighed with a Gaussian of standard deviation of one degree; the angular integration interval included 99.4% of the incident beam. The result of this treatment is displayed as A' and B' in Fig. 9. As expected, the spectra features are reduced and the FWHM increased. In addition, the minimum of the upper branch is shifted to a lower frequency by 3 cm^{-1}. This shift is caused by the shape of the upper branch in the reflectance surface. The shift is somewhat unpredictable as can be seen by another integration done for a gap spacing of 8.0 μm for which the minimum shifts upward 3 cm^{-1}. For measurements at smaller angles where the dispersion curve is near the light line, the minimum shift is reduced, but the amount is difficult to predict without this integration. Any attempt to include a non-uniform gap spacing would require a finite width beam treatment or the ATR technique which we did not attempt.[28] This underscores the requirement that the experimental conditions be rigidly controlled in order to plot dispersion curves from the ATR spectra.

IV. DISCUSSION

Barker and Loudon[4] have presented an alternative

approach for bulk polaritons which has been extended by Barker[29-31] to SEW. In analogy with mechanical systems they define a response function which governs the response of an oscillatory system to an applied force. The poles in the response function indicate the location of the normal modes of the system, while the shape of the function along the real plane is determined by the damping of the system. In this way one need only consider if his experiment measures ω complex with k_x real or ω real with k_x complex in order to decide the path on the response function surface. For an ATR experiment (with vacuum interface), Barker finds the response function to be of the form[30]

$$T(\omega,k) = [-\varepsilon(\omega)-\{[1-\varepsilon(\omega)k^2]/[1-k_o^2]\}^{1/2}]^{-1} \qquad (4)$$

where $k_o = (\omega/c)k$. At the pole in T, the dispersion relation is regained

$$k^2 = (\omega/c)^2\{\varepsilon/(\varepsilon+1)\} \qquad (5)$$

which will demonstrate bend back for real ω as we have shown. Since this response function is for the system without the prism, the response function is simply related to the ATR reflectivity only for large gap spacings where the influence of recoupling is small. Then

$$1-R \propto \mathrm{Im}[T(\omega)] \qquad (6)$$

where R is the ATR reflectivity. An additional disadvantage is that the variables are k and ω instead of experimental variables θ and ω. Although not explicitly mentioned by Barker, the T surface will also give bend back if ω is kept fixed and θ varied. The reflectivity R calculated from Wolter's equations can be thought of as the response function for SEW including the prism.

V. CONCLUSION

The ATR surface has been used to show how dispersion curves for surface electromagnetic waves with or without bend back can be obtained from measurements of ATR spectra. Theoretically, no bend back occurs if the dielectric function is purely real. The introduction of an imaginary part of the dielectric function complicates the picture because the poles now occur for complex values of k and ω. If one makes k_x real and ω complex, bend back does not occur, while complex k_x and real ω produces bend back in the dispersion curves. The ATR reflectivity surface then shows the relation between these two choices. Also, the problem of defining what is meant by an SEW becomes difficult because the decay of the fields away from the surface into the medium is always exponentially damped. In fact, dips may appear in the ATR spectrum where there

is no SEW, at least according to the usual criterion found without damping. This will be illustrated in a future paper.[5]

In addition the qualitative effect of a divergent incident beam can be visualized by considering the shape of the minima in the surface. A quantitative example is given for InSb with two gap spacings, and the shift in the upper branch minimum is shown to be toward higher frequency for one gap and toward lower frequencies for another.

The application of the reflectance surface technique is not limited to isotropic materials, and we will publish theoretical and experimental results for MnF_2 in a forthcoming paper.[5]

FIGURE CAPTIONS

Fig. 1. Dispersion curves for a 340 A silver film on a CaF_2 prism. Solid curve, obtained from cross section of the ATR reflectance surface for fixed frequencies. This solid curve also results from solving Eq. (1) using complex k_x and $\varepsilon(\omega)$. Dash-dot line, from cross sections for fixed angle. This dash-dot curve also results from solving Eq. (1) with $\varepsilon(\omega)$ purely real or with ω complex and k real. Crosses are experimental points of Arakawa, et al. (ref. 20) who fixed the frequency and varied the angle.

Fig. 2. The ATR reflectance of a 340 A thick Ag film on a CaF_2 prism plotted as a function of the incident frequency ω and the angle of incidence θ. Inset, ATR geometry of a prism or semicylinder (index of refraction n_p) with a silver film and a second interface with another medium.

Fig. 3. (a) Cross sections of the ATR reflectance surface of Fig. 2 obtained by holding the angle of incidence fixed and varying the incident frequency. The solid line is $\theta = 52°$, dashed is $\theta = 54°$, dashed dot is $\theta = 58°$ and dash-hatch is $\theta = 60°$. (b) cross sections of the ATR reflectance surface of Fig. 2 obtained by holding the incident frequency fixed and varying θ. The solid line is incident frequency of 3.4 eV and the

dash-hatch line is 3.7 eV. Note how the minimum in Fig. 3a move toward higher frequencies as θ increases while the last minimum moves back towards smaller θ (and hence smaller k_{1x}).

Fig. 4. ATR geometry with air gap. The incident light intensity is I_o, the reflected light intensity, I, the reflectance is I/I_o, θ is the incident angle in the hemicylinder prism, and d is the air gap spacing. The absorber is the material supporting the SEW and having a complex dielectric constant $\varepsilon(\omega) = \varepsilon_1(\omega) + i\varepsilon_2(\omega)$.

Fig. 5. ATR reflectance surface of NaCl with a 5.0 μm air gap spacing. The frequencies along the lower axis are 150 cm^{-1} to 250 cm^{-1}. The incident angles along the upper axis are 20° to 60°.

Fig. 6. ATR reflectance surface of NaCl with a 12.0 μm air gap spacing the frequencies along the lower axis are 150 cm^{-1} to 250 cm^{-1}. The incident angles along the upper axis are 20° to 60°.

Fig. 7. Dispersion curves of NaCl obtained from the ATR reflectance surface minima. The inset is a detailed view. The solid lines B and C are plotted from the cross sections with frequency fixed; the dashed curves B and C are plotted from cross sections with incident angle fixed. Curve B is from the reflectance surface of Fig. 5 with a

5.0 μm gap spacing. Curve C is from a reflectance surface with a 2.0 μm spacing. The triangles correspond to the 12.0 μm gap reflectance surface of Fig. 6 and they are not connected by a line for clarity. Curve A is the dispersion relation Eq. (1) with $\varepsilon(\omega)$ complex (solid line) and $\varepsilon(\omega)$ purely real (dashed line). The crosses are experimental points of Bryksin, et al.[22] The straight line is the free space photon dispersion line.

Fig. 8. ATR reflectance surface of InSb with a 19.0 μm air gap spacing. The frequencies along the lower axis are 150 cm^{-1} to 250 cm^{-1}. The incident angles along the upper axis are 18° to 38°.

Fig. 9. θ = 22° cross section of the InSb ATR surface. A is the lower branch and B is the upper branch. The dashed line is for τ = 10 cm^{-1}. The solid line is for τ = 20 cm^{-1}. The crosses are the experimental points of Bryksin, et al.[26] The lower curves A' and B' are the integrated divergent beam results. The dashed line is for τ = 10 cm^{-1} and the solid line is for τ = 20 cm^{-1}. Note the break in the y-axis.

REFERENCES

† Research done under Air Force Office of Scientific Research under Grant No. AFOSR-74-2654.

1. R. W. Alexander, G. S. Kovener, and R. J. Bell, Phys. Rev. Lett. 32, 154 (1974).
2. A. Otto, Z. Physik 216, 398 (1968), and K. W. Chiu and J. J. Quinn, Nuovo Cimento 10B, 1 (1972).
3. R. H. Ritchie, Surf. Sci. 34, 1 (1973).
4. A. S. Barker, Jr. and R. Loudon, Rev. Mod. Physics 44, 18 (1972).
5. G. S. Kovener, R. W. Alexander, Jr., and R. J. Bell, to be published.
6. R. J. Bell, R. W. Alexander, Jr., W. F. Parks, and G. Kovener, Optics Comm. 8, 147 (1973).
7. M. Born and E. Wolf, Principles of Optics, (Pergamon Press, Oxford, 1970).
8. P. B. Johnson and R. W. Christy, Phys. Rev. B6, 4370 (1972).
9. R. W. Gammon and E. D. Palik, Bull. Am. Phys. Soc. 18, 426 (1973) and Private Communication.
10. K. L. Kliewer and R. Fuchs (Phys. Rev. 144, 495 (1966)) have solved the radiative modes of an ionic slab with damping for ω complex and k complex but not the surface or non-radiative modes with damping.
11. H. J. Benson and D. L. Mills, Phys. Rev. B1, 4835 (1970).

12. R. R. Alfano, J. Opt. Soc. Am. 60, 66 (1970).

13. R. R. Alfano and T. G. Giallorenzi, Optics Comm. 4, 271 (1971).

14. T. G. Giallorenzi, Phys. Rev. B5, 2314 (1972).

15. H. E. Puthoff, R. H. Pantell, B. G. Huth, and M. A. Chacon, J. App. Phys. 39, 2144 (1968).

16. H. Wolter, Handbuch der Physik, ed. S. Flugge, Vol. 24, p. 461 (Springer, Berlin 1956).

17. A. Otto, Phys. Stat. Sol. (b) 34, 523 (1973).

18. I. I. Reshina, Yu. M. Gerbstein, and D. N. Mirlin, Sov. Phys.-Solid State 14, 1104 (1972).

19. N. Marschall and B. Fischer, Phys. Rev. Lett. 28, 811 (1972).

20. E. T. Arakawa, M. W. Williams, R. N. Hamm, and R. H. Ritchie, Phys. Rev. Lett. 31, 1127 (1973).

21. A. Otto, Private Communication.

22. V. V. Bryksin, Yu. M. Gerbstein, and D. N. Mirlin, Phys. Stat. Sol. (b) 51, 901 (1972).

23. This presents a problem in experimentally observing the SEW in anisotropic materials if one is attempting to locate the branches which terminate. This will be discussed in a future paper.

24. N. Marschall, B. Fischer, and J. J. Queisser, Phys. Rev. Lett. 27, 95 (1971).

25. W. E. Anderson, R. W. Alexander, Jr., and R. J. Bell, Phys. Rev. Lett. 27, 1057 (1971).

26. V. V. Bryksin, D. N. Mirlin, and I. I. Reshina, Sol. Stat. Comm. 11, 695 (1972).

27. H. Y. Fan in Optical Properties of III-V Compounds, ed. R. K. Willardson and A. C. Beer (Academic, New York, 1967).

28. J. Picht, Ann. d. Physik (5) 3, 433 (1929).

29. A. S. Barker, Jr., Phys. Rev. Lett. 28, 892 (1972).

30. A. S. Barker, Jr., Surf. Sci. 34, 62 (1973).

31. A. S. Barker, Jr., Phys. Rev. B8, 5418 (1973).

TABLE I

NaCl Oscillator Parameters

ω_i (cm^{-1})	$\delta\varepsilon_i$	Γ_i (cm^{-1})
164	3.1975	6.13
247	0.0898	34.7

$\varepsilon_\infty = 2.32$

TABLE II

InSb Oscillator Parameters

$\omega_t (cm^{-1})$	179	$N(cm^{-3})$	2.00×10^{17}
$\delta\varepsilon$	2.0	m*	$0.022\ m_e$
$\Gamma (cm^{-1})$	2.864	$\tau (cm^{-1})$	10.0
ε_∞	15.7		

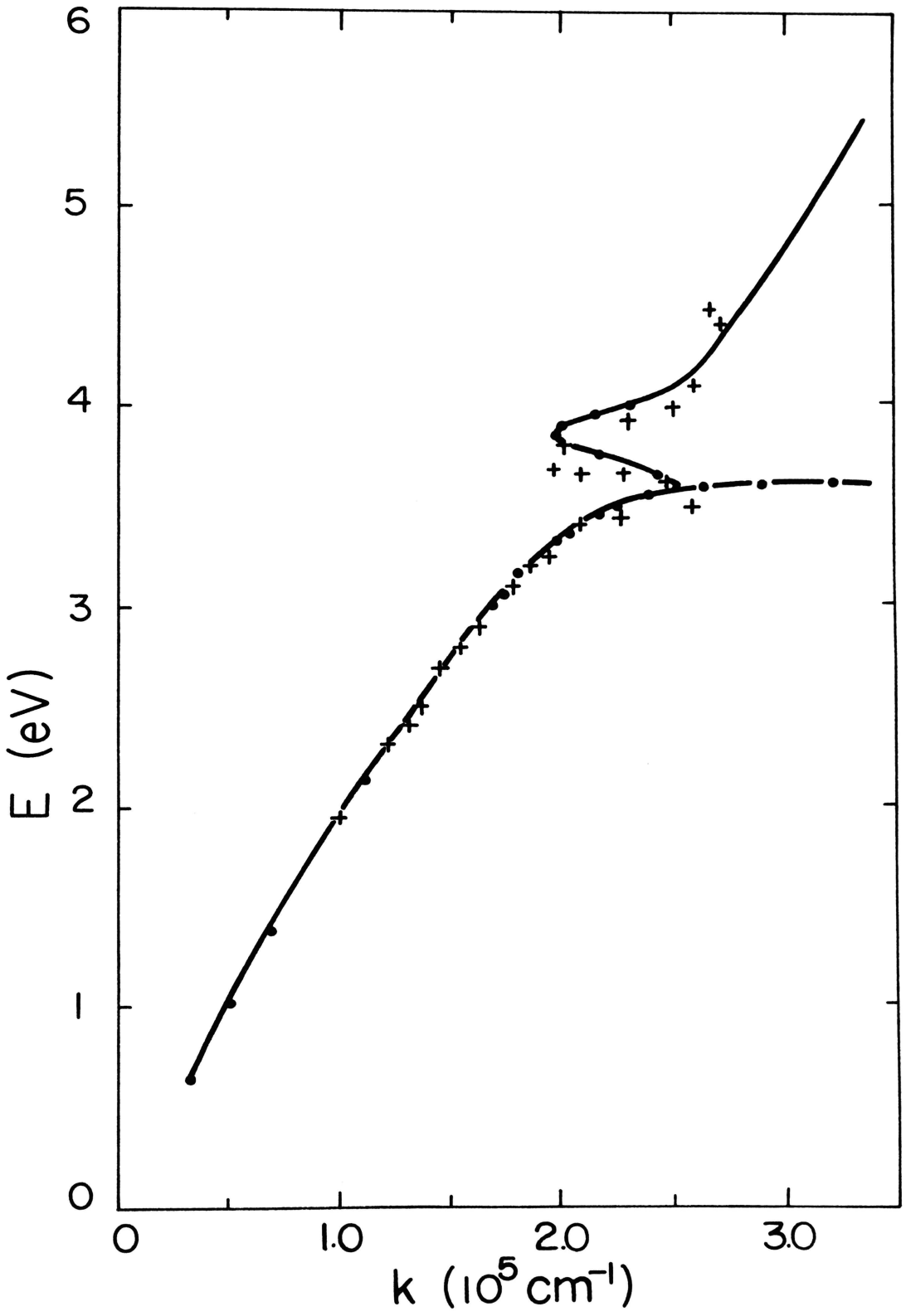

Figure 1.

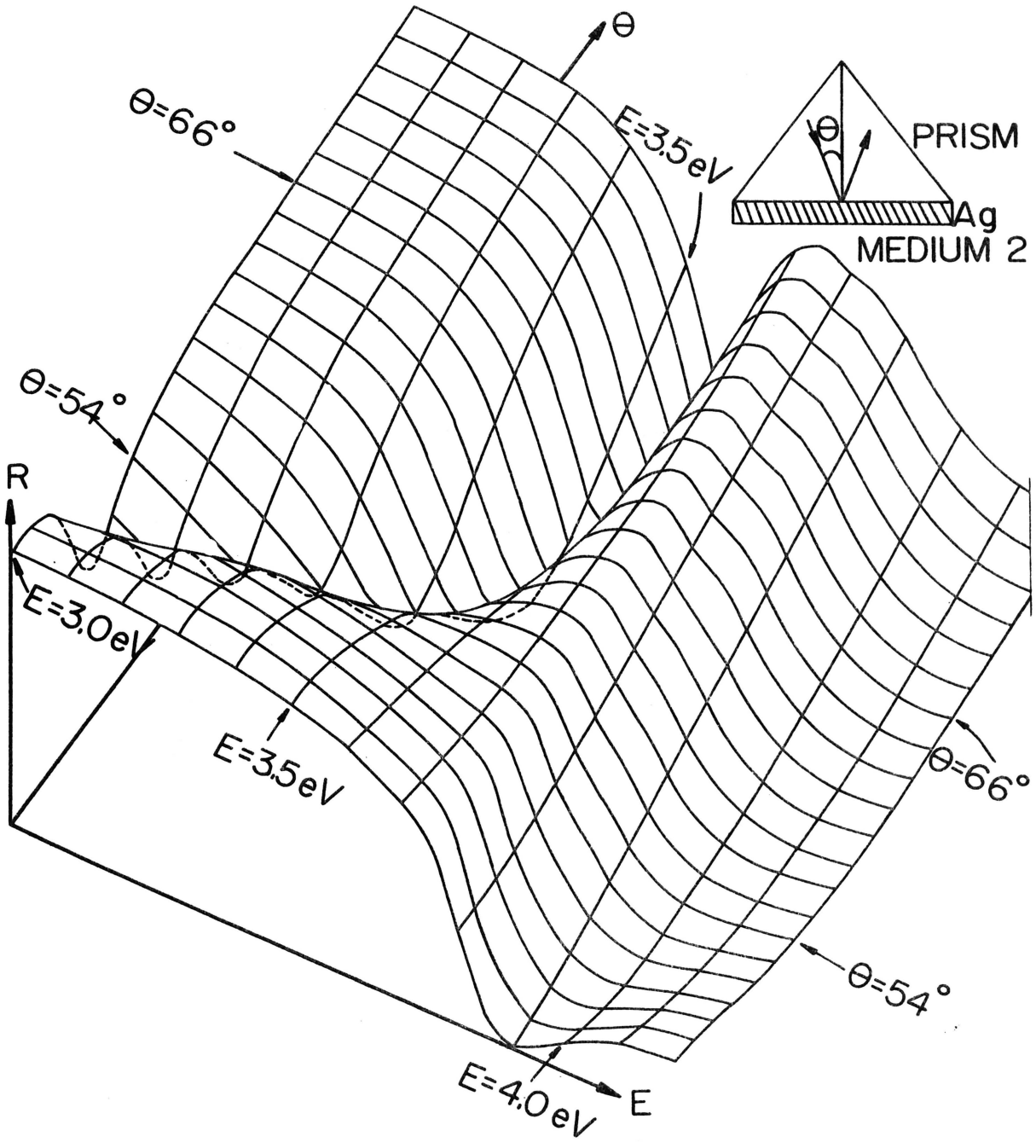
Θ
Θ=66°
E=3.5eV
Θ
PRISM
Ag
MEDIUM 2
Θ=54°
R
E=3.0eV
E=3.5eV
Θ=66°
Θ=54°
E=4.0eV
E

Figure 2.

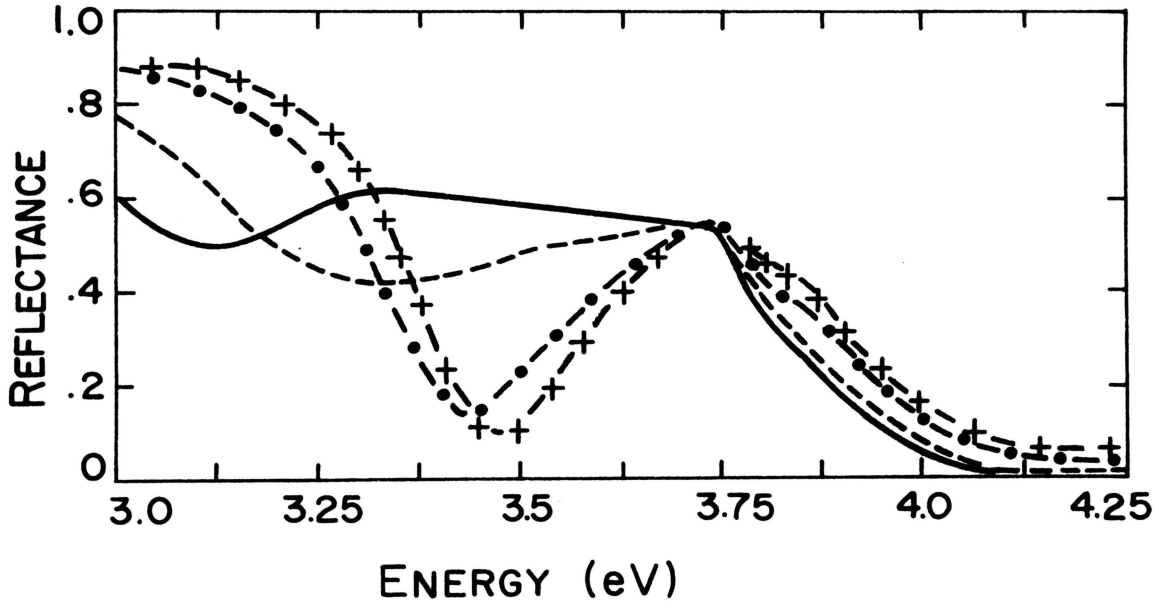

Figure 3a.

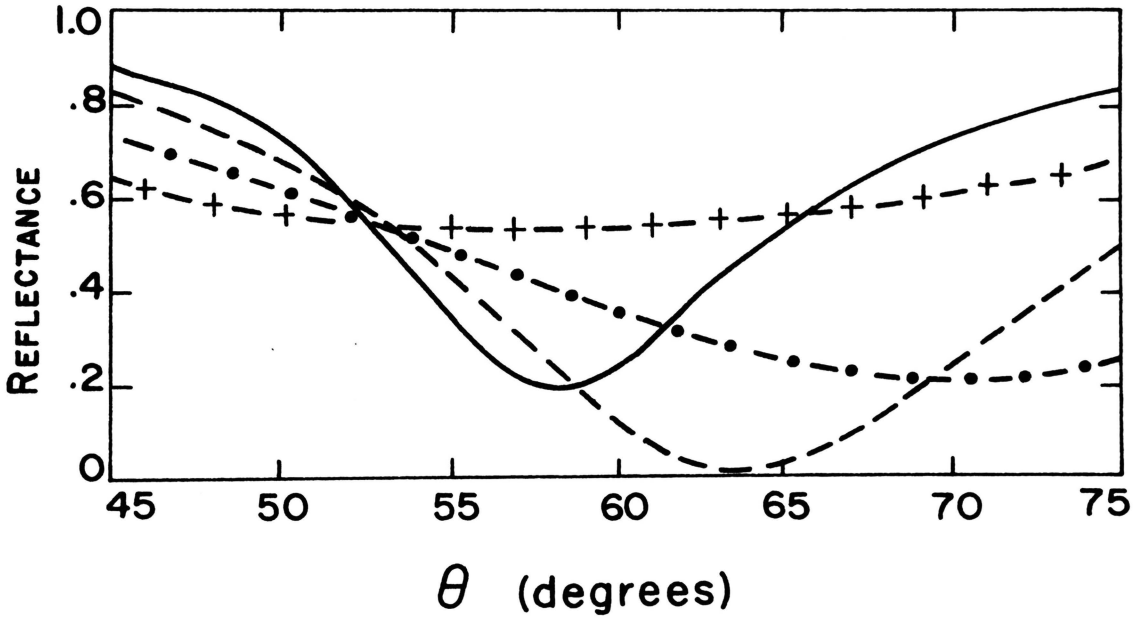

Figure 3b.

ATR GEOMETRY

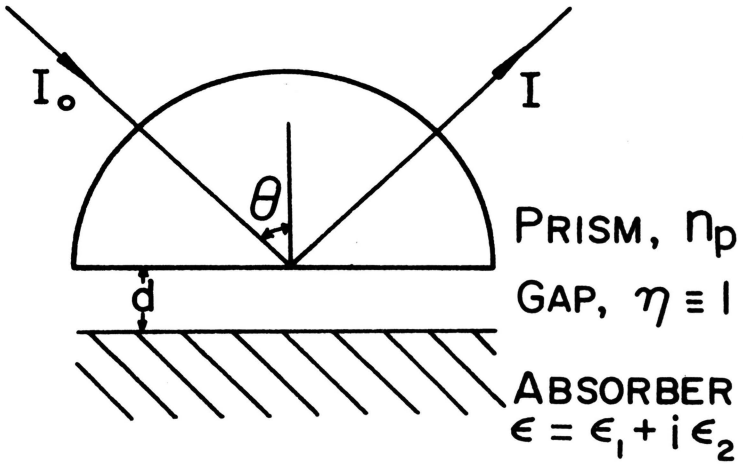

Figure 4.

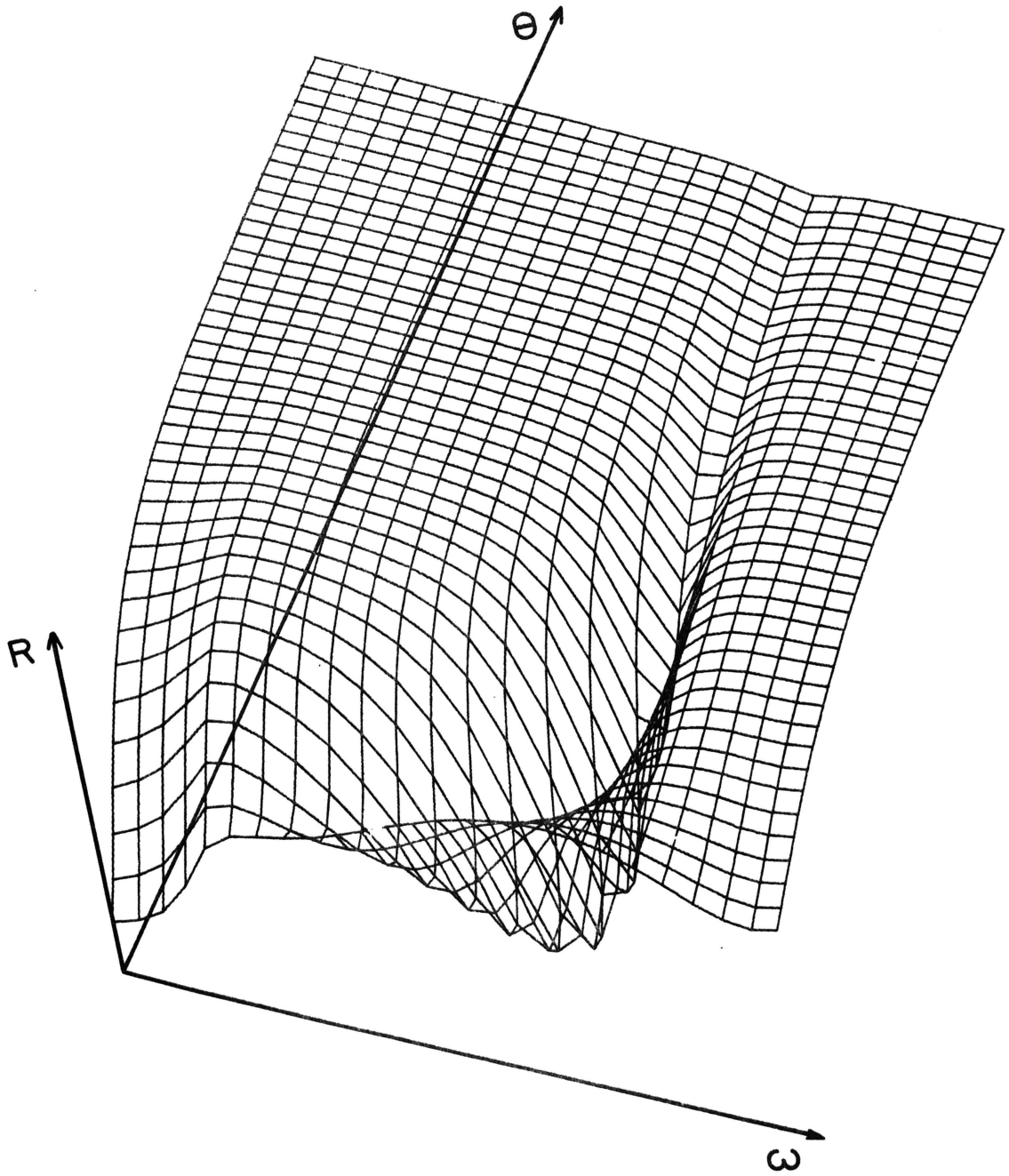

Figure 5.

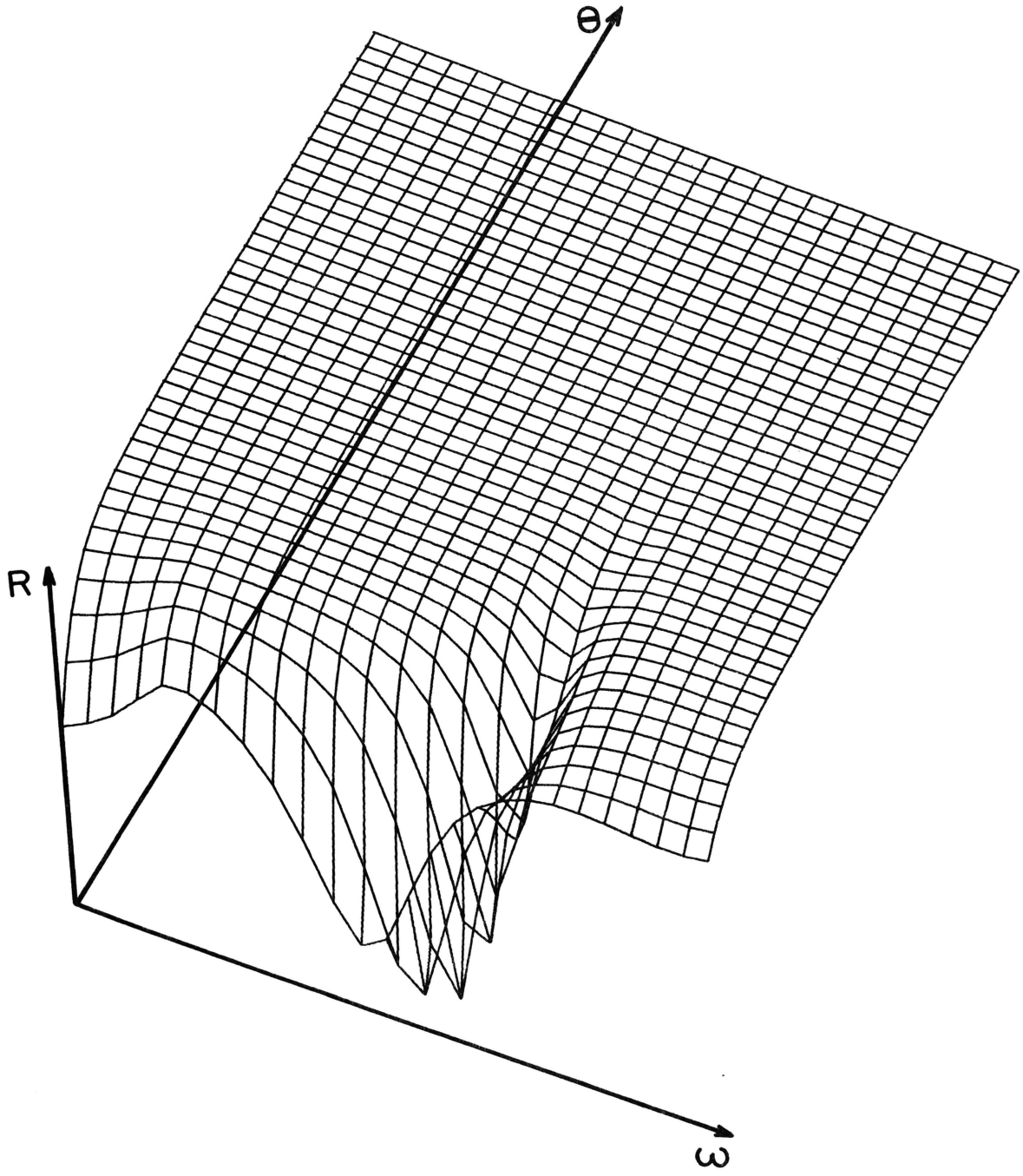

Figure 6.

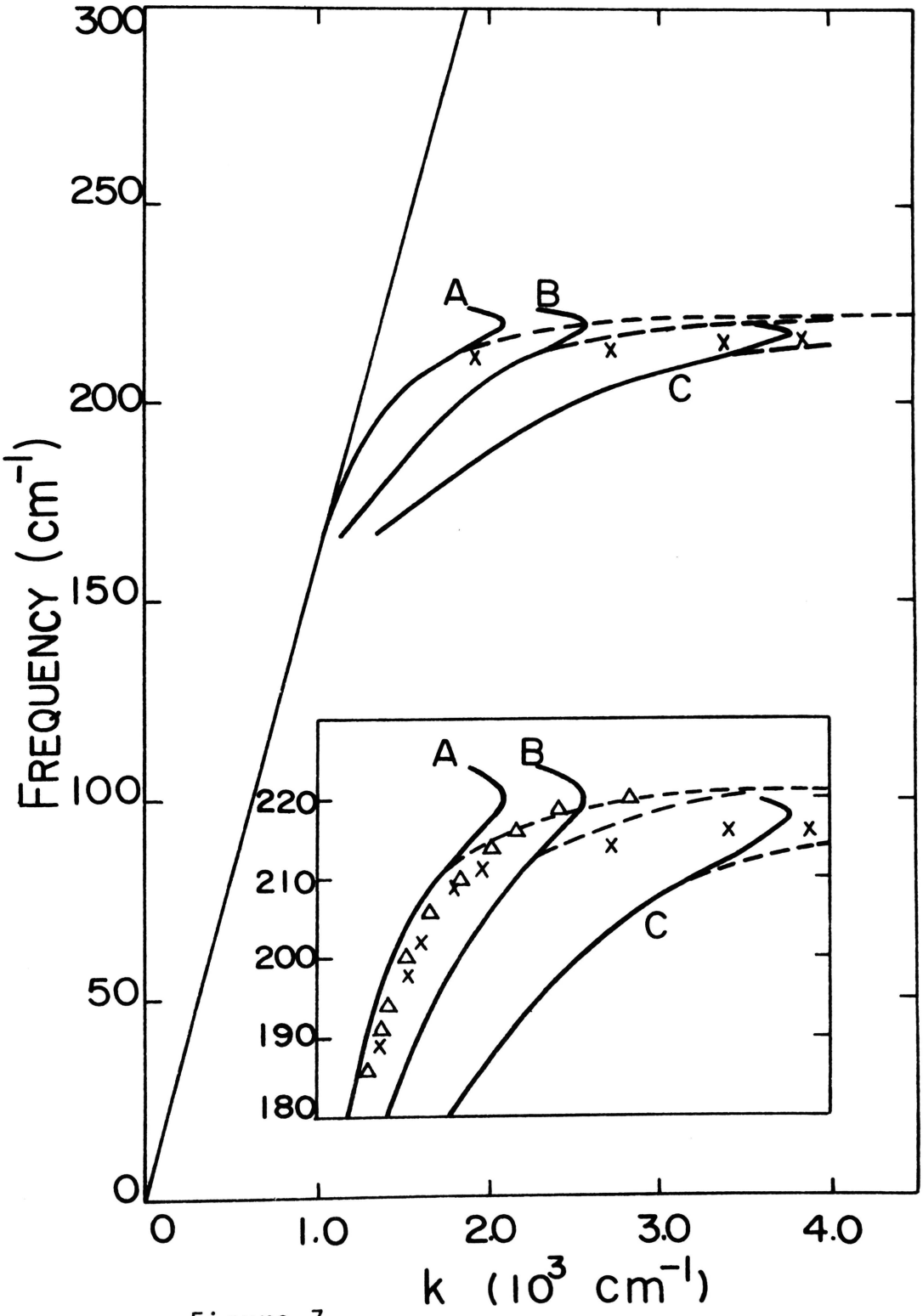
300
250
200
150
100
50
0
FREQUENCY (cm⁻¹)
A
B
C
0
1.0
2.0
3.0
4.0
k (10³ cm⁻¹)
220
210
200
190
180

Figure 7.

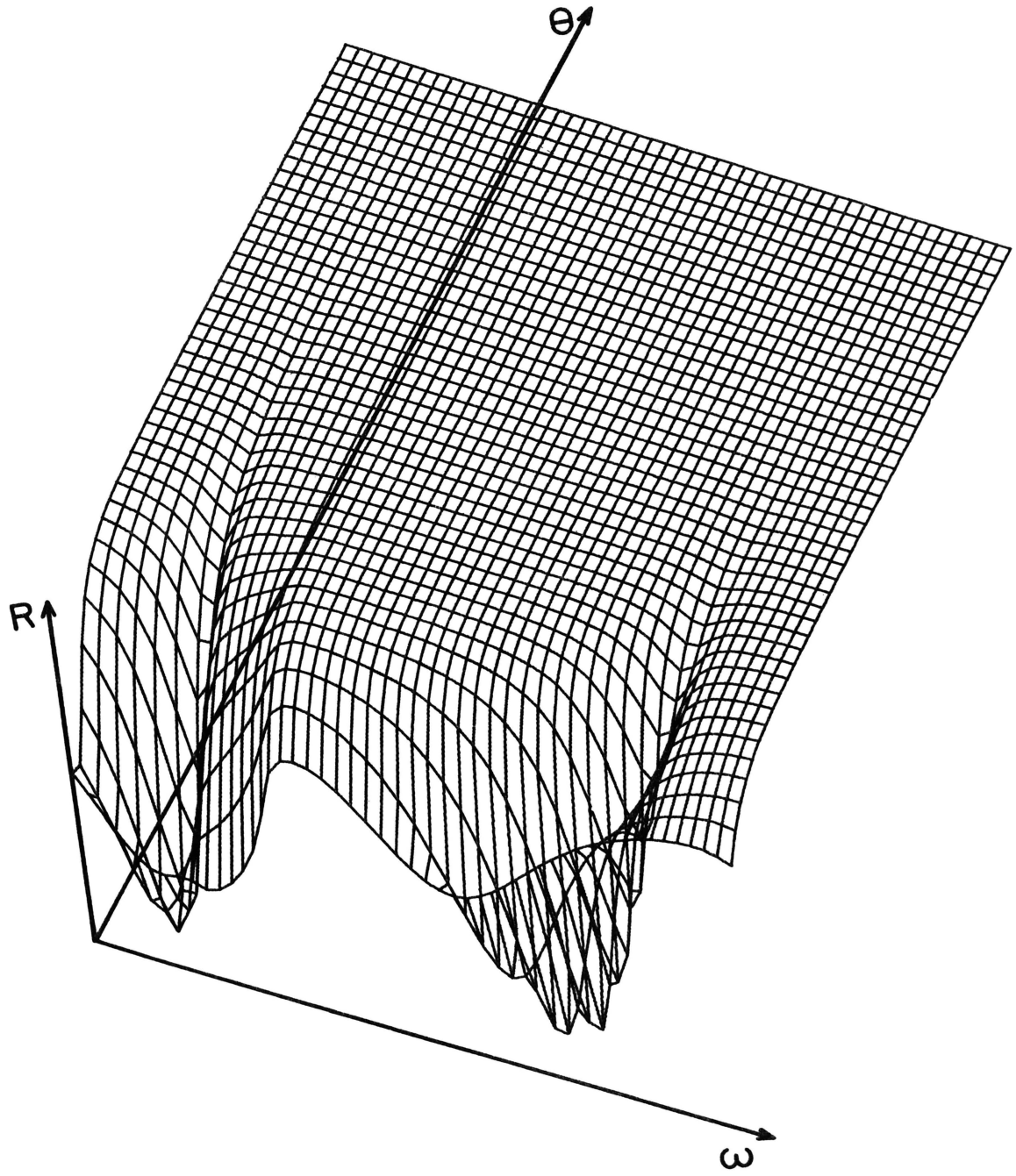

Figure 8.

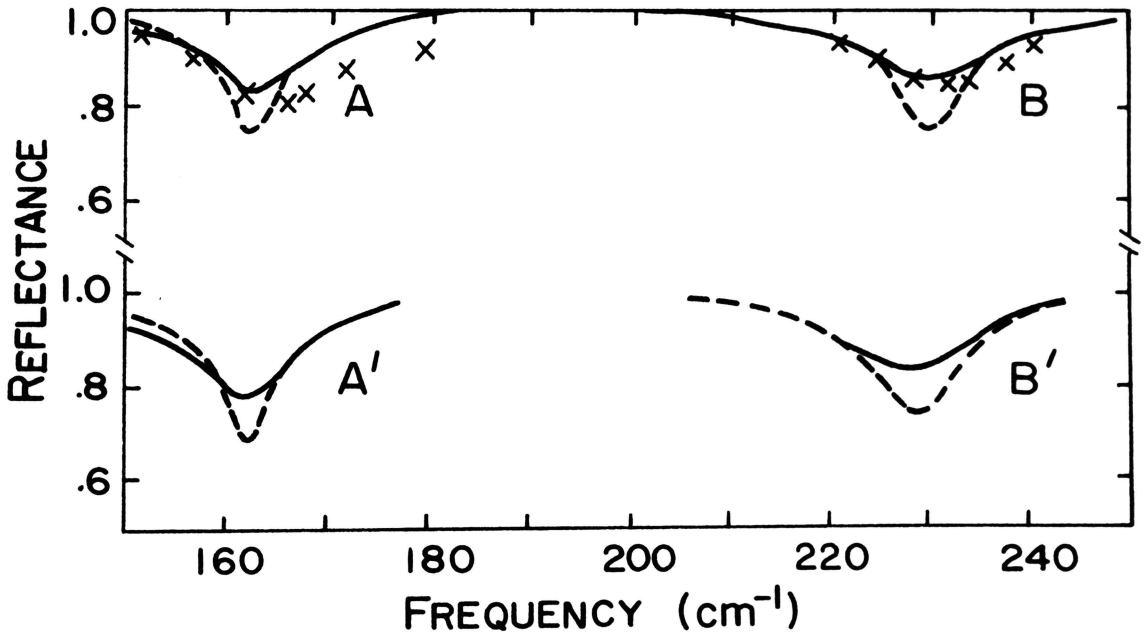
1.0
.8
.6
1.0
.8
.6
REFLECTANCE
A
B
A′
B′
160
180
200
220
240
FREQUENCY (cm⁻¹)

Figure 9.

ACKNOWLEDGEMENTS

We would like to thank Ms. C. A. Ward for her programming.

ATR REFLECTIVITY STUDY OF SURFACE ELECTROMAGNETIC WAVES ON ANISOTROPIC MATERIALS WITH DAMPING†

by

G. S. Kovener, R. W. Alexander, Jr.,
I. L. Tyler, and R. J. Bell

Graduate Center for Materials Research
and Physics Department
University of Missouri-Rolla
Rolla, Missouri 65401

ABSTRACT

The technique of plotting the ATR reflectance as a function of both frequency and incident angle using a three dimensional plot is applied to surface electromagnetic waves (SEW) in a uniaxial material, MnF_2. It is shown that dispersion curves calculated without absorption do not completely describe the ATR reflectivity. Experimental data confirming the reflectance surface features are presented. The termination of an extraordinary SEW dispersion branch is observed experimentally, and the experimental conditions for this observation are discussed. Also, additional minima in the reflectance surface not associated with SEW are found.

I. INTRODUCTION

The three dimensional ATR reflectance surface technique has been previously applied to isotropic materials in order to explain various aspects of the ATR spectra including the bend back behavior of the surface electromagnetic wave (SEW) dispersion curves.[1,2] This technique of plotting reflectance as a function of both frequency and incident angle can be used for anisotropic materials, and we present a treatment of the attenuated total reflection (ATR) spectra for MnF_2, a uniaxial material, using the reflectance surface technique. The ambiguity present in identifying all minima in the ATR spectra as SEW minima will be discussed.

We have experimentally measured several branches of the SEW dispersion curves of MnF_2, and these results will be discussed. In addition, the termination of a dispersion curve branch has been observed. Several other features predicted by the reflectance surface approach to SEW have been confirmed experimentally.

II. THEORY

The description of SEW on anisotropic materials was first presented by Lyubimov and Sannikov[3] although surface magnetoplasmons which have a uniaxial dielectric tensor were treated earlier.[4-7] For non-magnetic anisotropic

materials, the first experimental observations of SEW using the ATR technique of Otto[8] were made by Bryksin, Mirlin and Reshina[9,10] on MgF_2 and TiO_2, followed by Falge and Otto[11] on quartz and by Perry, Fischer, and Buckel on Cds.[12]

In order to properly discuss SEW in anisotropic materials, the theory of Lyubimov and Sannikov will be reviewed and then the dispersion relations will be examined. In this paper, we will consider only non-magnetic media which are not optically active. Since the experimental data was taken for MnF_2, we will further consider only uniaxial materials and refer the reader to Burstein, et al. for a treatment of biaxial crystals.[13]

Rather than reproducing a complete description of the Lyubimov and Sannikov derivation of SEW dispersion relations in anisotropic materials, only the important points of departure from the isotropic case will be mentioned. For uniaxial materials, the electric fields can be divided into ordinary and extraordinary components based on the orientation of E relative to the plane containing k and the optic axis (OA). Choosing the z axis normal to the crystal surface and the optic axis at an angle θ relative to the surface, the bulk dispersion relations are:

$$k_o^2 + k_{zo}^2 = \varepsilon_\perp(\omega) \qquad (1a)$$

$$(k_e^2 + k_{ze}^2)\varepsilon_\perp(\omega) + (k_x \sin\theta + k_{ze}\cos(\theta))^2(\varepsilon_{||}(\omega) - \varepsilon_\perp(\omega))$$
$$= \varepsilon_{||}(\omega)\varepsilon_\perp(\omega) \qquad (1b)$$

where k_o and k_e are the ordinary or extraordinary wavevectors parallel to the surface, and k_{zo} and k_{ze} are the ordinary and extraordinary wavevector components normal to the surface. $\varepsilon_{||}(\omega)$ and $\varepsilon_\perp(\omega)$ are the dielectric tensor components relative to the optic axis. If only the three special orientations of Fig. 1 are considered, then the Maxwell boundary conditions at the z = o plane are simplified since each case has only one E field present for p - polarized radiation. Cases I and II have only extraordinary E fields and Case III has only ordinary E fields. Applying the boundary conditions and the bulk dispersion relations of Eq. (1), dispersion solutions are obtained which are characterized (in the absence of damping) by a propagating wave along the interface and damped fields normal to the interface.

For these special orientation of the optic axis, propagation vector, and the crystal surface, the dispersion relations are simplified to the equations shown in Fig. 1 where OA is the optic axis direction or the direction of the axis of rotational symmetry. With a first consideration of the two unequal dielectric tensor components, one would expect just two different dispersion relations. However, Maxwell's boundary conditions applied

to the crystal surface distinguish between Case I and Case II. We will use Lyubimov and Sannikov's notation in calling Case I and Case II extraordinary SEW and Case III ordinary SEW. The dispersion relations for the three cases are:[3]

$$\text{Case I} : \quad k_x = (\omega/c)[(\varepsilon_{\parallel}\varepsilon_{\perp}-\varepsilon_{\parallel})/(\varepsilon_{\parallel}\varepsilon_{\perp} - 1)]^{1/2} \tag{2a}$$

$$\text{Case II} : \quad k_x = (\omega/c)[(\varepsilon_{\parallel}\varepsilon_{\perp}-\varepsilon_{\perp})/(\varepsilon_{\parallel}\varepsilon_{\perp} - 1)]^{1/2} \tag{2b}$$

$$\text{Case III}: \quad k_x = (\omega/c)[\varepsilon_{\perp}/(\varepsilon_{\perp} - 1)]^{1/2} \tag{2c}$$

For the purpose of demonstrating the problems associated with using damping in the dielectric function, let us first examine Eq. (2a) with purely real dielectric functions $\varepsilon_{\parallel}(\omega)$ and $\varepsilon_{\perp}(\omega)$ i.e., no damping included. For an excitation to be defined as a SEW, k_x must be real and

$$k_x > (\omega/c). \tag{3}$$

In addition, the values of k_z in each medium must be appropriate to lead to real exponential decay of the fields as $z \to \pm \infty$. If k_z in the vacuum is labeled k_{gz} and k_z in the materials as k_{az}, then for fields of the form $\exp[-i(k_z z)]$ (see Appendix), one obtains

$$k_x = (\omega/c)[(\varepsilon_{\parallel}\varepsilon_{\perp} - \varepsilon_{\parallel})/(\varepsilon_{\parallel}\varepsilon_{\perp} - 1)]^{1/2} \tag{4a}$$

$$k_{az} = (\omega/c)[\varepsilon_{\perp}^{2}(\varepsilon_{\parallel} - 1)/(\varepsilon_{\parallel}\varepsilon_{\perp} - 1)]^{1/2} \tag{4b}$$

and

$$k_{gx} = (\omega/c)[(\varepsilon_{\parallel} - 1)/(\varepsilon_{\parallel}\varepsilon_{\perp} - 1)]^{1/2} \tag{4c}$$

Since k_{az} and k_{gz} must be imaginary for damping and the imaginary parts of each must be of opposite sign as $z \to \pm \infty$, then

$$\text{IMAG}(k_{az})/\text{IMAG}(k_{gz}) = \varepsilon_{\perp}(\omega) < o \tag{5}$$

Therefore $\varepsilon_{\perp}(\omega)$ must be negative for Case I SEW to exist.

The other component of the dielectric tensor $\varepsilon_{\parallel}(\omega)$ must also be examined. There are four regions to consider:

$$1: \quad \varepsilon_{\parallel}(\omega) < o, \ \varepsilon_{\parallel}(\omega)\varepsilon_{\perp}(\omega) > 1 \tag{6a}$$

$$2: \quad \varepsilon_{\parallel}(\omega) < o \quad \varepsilon_{\parallel}(\omega)\varepsilon_{\perp}(\omega) < 1 \tag{6b}$$

$$3: \quad 1 > \varepsilon_{\parallel}(\omega) > o \tag{6c}$$

$$4: \quad \varepsilon_{\parallel}(\omega) > 1 \tag{6d}$$

It is a simple matter to show that only region 1 and region 4 satisfy the conditions on k_x, k_{gz}, and k_{az}. In region 1, $k_x \to \infty$ as the frequency approaches a limiting ω_s given by

$$\varepsilon_{\parallel}(\omega_s)\varepsilon_{\perp}(\omega_s) = 1. \tag{7}$$

Except for the presence of the additonal dielectric function, the asymptotic behavior of the dispersion curve is the same as that of isotropic dispersion curves for

similar dielectric functions. For region 4, the wave-vector k_x does not approach large values but terminates at a finite value given by

$$k_B = (\omega/c)\sqrt{\varepsilon_{\parallel}} \quad . \tag{8}$$

This is the bulk polariton dispersion relationship and the SEW changes into a bulk wave at k_B. This behavior is unique to anisotropic materials. A similar analysis can be made for Case II by interchanging $\varepsilon_{\parallel}(\omega)$ and $\varepsilon_{\perp}(\omega)$. Case III has a dispersion relation identical to that of isotropic SEW and those results apply here; specifically, SEW exist for $\varepsilon_{\perp}(\omega)<-1$ and $k_x \to \infty$ as $\omega \to \omega_s$ given by

$$\varepsilon_{\perp}(\omega_s) = -1 \tag{9}$$

The dispersion relations (Eqs. 2) were originally derived for real $\varepsilon_{\parallel}(\omega)$ and $\varepsilon_{\perp}(\omega)$, i.e., no damping. Bryksin, et al.[10] have shown that the form of the dispersion curve is the same when $\varepsilon_{\parallel}(\omega)$ and $\varepsilon_{\perp}(\omega)$ become complex. However, a problem similar to that for isotropic materials occurs. For ω real, k_x must be complex from Eq. (2). This leads to bend back exactly as in the isotropic case[1,2]. Although we have not attempted the solution of Eq. (2) for ω complex and k_x real, there is no apparent reason for it to differ from the isotropic case for which k_x approaches infinity as $\omega \to \omega_s$. This discrepancy can

be treated using the ATR reflectance surface technique just as in the isotropic case, and we will discuss this technique later in this paper.

There are additional problems associated with complex $\varepsilon_{\parallel}(\omega)$ and $\varepsilon_{\perp}(\omega)$. In the discussion of regions in which we expect SEW, it was shown that $\varepsilon_{\perp}(\omega)<o$ and $\varepsilon_{\parallel}(\omega)\varepsilon_{\perp}(\omega)>1$ by requiring the k_{az} and k_{gz} be imaginary for proper decay of the fields. Now of course, this is meaningless since for any complex dielectric constant, k_{az} will be complex and will lead to decay of the field. Bryksin, Mirlin, and Reshina[10] proposed using just the real part of $\varepsilon_{\parallel}(\omega)$ and $\varepsilon_{\perp}(\omega)$ but as we shall see, this leads to inconsistencies in the assignment of SEW to minima in the ATR spectra.

This point is best illustrated by considering the dielectric function of MnF_2. Using the three phonon model parameters for $\varepsilon_{\parallel}(\omega)$ and the three phonon model parameters for $\varepsilon_{\perp}(\omega)$ as given by Weaver, et al.[14] and summarized in Table I, the real part of $\varepsilon(\omega)$ is plotted in Fig. 2. Note the small peak at 244 cm^{-1}. This is due to the resonance at 254.1 cm^{-1}, but this oscillator strength is not sufficient to force the real part of $\varepsilon_{\perp}(\omega)$ to be negative. Therefore no SEW should exist; yet, with no damping $\varepsilon_{\perp}(\omega)$ (which is now real) is negative and a SEW should exist. An inconsistency is present at this frequency regarding the presence or absence of a SEW

while in fact a minimum was observed in the experimental data near 258 cm^{-1}. We will discuss the experimental aspect in the next section. We will therefore define that Eqs. (2) are to be used only for $\varepsilon_{\parallel}(\omega)$ and $\varepsilon_{\perp}(\omega)$ purely real and the results will dictate which ATR minima will be defined as SEW minima.

As an aid in labeling the minima in the ATR spectra, the dispersion relations Eq. (2) are plotted in Fig. 3 using purely real dielectric functions. The dispersion branches for all orientations are presented in one graph; but, of course, only one case may be observed for a particular experimental configuration. The solid lines are Case I, the dash-dot lines are Case II, and the dashed lines are Case III. The arrows A indicate the maximum wavevector allowed for the extraordinary SEW as discussed earlier. For branch 2, the two Cases I and III are not sufficiently different in frequency to be separated on this scale. Note that there is no Case II extraordinary SEW until 280 cm^{-1}. The solid line labeled "light line" is the dispersion line of free space photons and the line labeled "silicon line" is the maximum wavevector available with a silicon ATR prism. Thus only one terminating branch, branch 1, would be accessible using a silicon prism. All three upper branches are asymptotic. It must be kept in mind, however, that purely real $\varepsilon_{\parallel}(\omega)$ and $\varepsilon_{\perp}(\omega)$ were used and this does not adequately describe

the SEW in a damped material.

There is no difficulty in the experimental results if the ATR reflectance surface technique is used to describe the experiment. Using uniaxial ATR reflectance equations derived in the Appendix, the reflectance can be plotted along the vertical axis as a function of ω and θ. Fig. 4 is a reflectance surface for MnF_2 with Case I orientation. The gap spacing is 2.0 μm, the frequency range is 100 cm^{-1} to 500 cm^{-1}, and the incident angle is 20 to 80 degrees. If an experimental ATR spectra is measured by fixing the incident angle and scanning the frequency, the results will follow a cross section going from left to right. Conversely if the ATR spectra is measured by fixing the frequency and scanning the incident angle, the results will follow a cross section going from bottom to top. This is discussed further elsewhere[1,2].

The reflectance surfaces for Case I, Case II, and Case III are shown in Figs. 4, 5, and 6 respectively. The gap spacing was 2.0 μm in all cases, and the ranges of frequency and incident angle are the same as those mentioned earlier. Some general comments can be made about all three cases. The dispersion of branch 3 can be seen as the turning of the "valley" toward lower ω as θ decreases. For a given ω, decreasing θ corresponds to decreasing k_x through the governing ATR equation

$$k_x = (\omega/c)\, n_p \sin(\theta) \qquad (10)$$

where n_p is the prism index of refraction. Notice that there is a maximum in the reflectivity at small angles near 200 cm^{-1}, and this maximum obscures the SEW minimum which is present at larger angles. Also note that the minima become quite shallow as θ gets larger and in fact at 70 degrees the minima are too small to be observed experimentally.

The last effect precludes observation of the branch 1 termination for Case I SEW since Eq. (8) and Eq. (10) indicate that θ would be 72 degrees. In order to increase the minima depth at larger angles, the gap spacing was reduced to 0.5 μm and the resulting surface for Case I is shown in Fig. 7. As θ increases, branch 1 now rises until it becomes a small, local maximum while the neighboring branch 2 continues to larger angles as a minimum. This is also apparent for this surface in the fixed angle cross sections which are displayed in Fig. 8. (The curves are offset for clarity). The other branches which terminate are not available with the silicon prism. In addition, the cross sections show the enhancement of the maximum at small angles which is due to the smaller gap. The complexity of the surfaces and their rapid change with different gap spacings indicate that the gap spacing must be uniform for quantitative ATR measurements,

especially at smaller gaps.

III. EXPERIMENTAL

The ATR spectra of MnF_2 were measured using a RIIC FS-720 Michelson Fourier transform spectrometer with a Golay cell detector. The data was obtained by fixing the angle and "scanning" the frequency. In most cases the apodized resolution was 2.0 cm^{-1} and the uncertainty in the incident angle was ± 2.0 degrees. A sample holder for use with the RIIC TR-5 Micro ATR unit was fabricated to press the silicon (n_p = 3.418) hemicylinder prism against the crystal. The gap spacing was provided by Mylar spacers (2.0 μm) or if smaller gaps were required, the prism was pressed directly against the sample. The spacing was estimated using visible light interference fringes. The crystals were purchased from Optovac, Inc. and the surfaces were polished to 1/4 λ (Na) flatness over a minimum of 80% of the surface. We have found that a large area must be flat in order to couple effectively (the incident beam diameter was approximately 5 mm). One face had the optic axis normal (basal face) and one face had the optic axis parallel to an edge (CA face). Since MnF_2 is a transparent uniaxial material, the orientation of the crystal is easily decided with crossed polarizers. The beam divergence inside the prism was estimated to be

1.0 degree. All data was taken at room temperature. The relative reflectance was determined by a ratio of the ATR reflectance with MnF_2 to the ATR reflectance with a polished Al cube substituted for the crystal.

A representative experimental result is shown in Fig. 9 for Case I orientation. The gap was 1.0 μm and the incident angle $\theta = 30°$. The minimum at 206 cm^{-1} occurs at a frequency for which $\varepsilon_{\perp}(\omega)$ is negative (see Fig. 2), and we will assign it to the branch 1 extraordinary SEW. Note, however, that the second minimum at 259 cm^{-1} occurs at a frequency for which real $\varepsilon_{\perp}(\omega)$ is positive (see Fig. 2). We therefore assign this minimum to the branch 2 extraordinary SEW using the definitions carried over from the cases involving zero damping.

After converting the reflectance minima to wave-vector k_x using Eq. (10), the results are plotted in Fig. 10. The triangles are the data points for Case I and the squares for Case III. The solid line is the Case I dispersion relation Eq. (2a), and the dashed line is the Case III dispersion relation Eq. (2c). The data for Case III branch 1 was taken with a 2.0 μm gap spacing while the gap spacing was 0.5 μm for the Case III branch 2 data. The data for Case I was taken with a 0.5 μm gap. The experimental points are slightly lower in frequency than the theoretical values, but this is expected since smaller gaps do produce a shift toward lower frequency

minima in isotropic materials.

The termination of the Case I extraordinary SEW at point A was observed by noting the disappearance of the branch 1 while the branch 2 remained for increasing angles. The experimental spectra are displayed in Fig. 11. The minimum disappeared at an experimental incidence angle of 60° which was less than the 72° predicted by the dispersion curves without damping. This discrepancy is due to the finite divergence of the incident beam, and the subjective choice of when the minimum has "disappeared".

Qualitative agreement with the calculated ATR reflectance surface and the empirical data of Case III can be seen in the Fig. 12 for a gap of 0.5 μm where the reflectivity is decreased at 125 cm^{-1} for the small angle. Then as θ is increased, the experimental reflectivity in this 125 cm^{-1} region increases. Furthermore branch 1 is not apparent in the smaller angle spectra. At 0.5 μm the minimum is shifted to 185 cm^{-1} (from 200 cm^{-1} at 2 μm) because of the smaller gap.

Examining the reflectance surface of Fig. 6, one can see that this minimum disappears at smaller angles due to the large increase in reflectivity centered on 185 cm^{-1} for small angles. The existence of this "bump" is then confirmed experimentally.

In Case II the ATR spectra pointedly indicates the difficulties associated with using the dispersion relation

Eq. (2b). As one can see in the reflectance surface (Fig. 5) and the fixed angle cross section in Fig. 13, a pronounced minimum occurs at 250 cm^{-1} and yet even $\varepsilon_{\parallel}(\omega)$ with no damping is positive. By our previous definition of SEW minima, this cannot be assigned to a SEW. The extraordinary SEW predicted from Eq. (2b) is the small dip at 280 cm^{-1} in the calculated cross section (Fig. 13). Our experimental data were not sufficiently good to detect this small minimum. Similar observational difficulties were also encountered by Bryksin, et al.[10] with MgF_2 which is structurally similar to MnF_2.

CONCLUSION

Previous theoretical treatments of SEW on anisotropic materials which did not include absorption are shown to be inadequate. When the dielectric function is allowed to be complex so as to include absorption, the dispersion curves can be made to bend back or to show asymptotic behavior near the usual surface polariton frequencies. This problem with the dispersion curves has been previously noted for isotropic materials. In addition, the component of the wavevector normal to the surface as calculated from complex dielectric functions is always complex and the usual conditions for the existence of SEW are no longer precise.

To overcome these difficulties with complex dielectric functions the technique of displaying the ATR reflectance as a three dimensional plot of reflectance vs. both ω and θ can be used very effectively. Using this complete dielectric description of the anisotropic material, most minima or "valleys" in the surface can be assigned as SEW. Using the conditions of Eqs. (6a,d) with the real parts of $\varepsilon_{\parallel}(\omega)$ and $\varepsilon_{\perp}(\omega)$. Other minima exist at frequencies where $\varepsilon_{\parallel}(\omega)$ and $\varepsilon_{\perp}(\omega)$ satisfy Eqs. (6a,d) only if damping is omitted. A third type of minima occur where the conditions of Eqs. (6a,d) are not met, with or without damping. These three types of minima are all observed in the experimental measurements on MnF_2.

The termination of an extraordinary SEW was examined using the reflectance surface and experimental verification was found. With this graphical reflectance surface technique, we have demonstrated that a small gap is required to avoid confusing the termination with the normal reduction of the reflectivity minima as θ increases.

APPENDIX

The ATR reflectance for an anisotropic sample with absorption is derived for special orientations of k_x and the optic axis. The geometry is that of Fig. A1. Subscripts p., g., and a. refer to the prism, gap and absorber respectively. The prism is non-absorbing ($\varepsilon_p = n_p^2$), and the gap has dielectric constant ε_g. The three orientations considered are those shown in Fig. 1 and the incident light is p-polarized.

The electric fields are written (with time dependence $e^{-i\omega t}$) in the three regions as:

$$\text{prism} \quad : \quad \vec{E}_p = \xi_{1p}(1,0,k_x/k_{pz})\exp[i(k_x x - k_{pz} z)] + \xi_{2p}(1,0 - k_x/k_{pz})\exp[i(k_x x + k_{pz} z)] \qquad \text{(i)}$$

$$\text{gap} \quad : \quad \vec{E}_g = \xi_{1g}(1,0,k_x/k_{gz})\exp[i(k_x x - k_{gz} z)] + \xi_{2g}(1,0, - k_x/k_{gz})\exp[i(k_x x + k_{gz} z)] \qquad \text{(ii)}$$

$$\text{absorber:} \quad \vec{E}_a = \xi_{1a}(1,0,A)\exp[i(k_x x - k_{az} z)] \qquad \text{(iii)}$$

The first term in Eq. (i) is the incident beam and the second term is the reflected beam. Thus we want to determine the reflectance ratio $r = \xi_{2p}/\xi_{1p}$. The coefficient A depends upon the orientation of $\vec{k}$ and the optic axis, and will be determined from $\nabla \cdot \vec{D} = 0$. We shall require $\text{Imag}(k_{az}) > 0$ so that the field decays as $z \to -\infty$.

The dielectric tensor is diagonal and has the following forms for the three cases considered.

Case I

$$\underline{\underline{\varepsilon}} = \begin{bmatrix} \varepsilon_\perp & 0 & 0 \\ 0 & \varepsilon_\perp & 0 \\ 0 & 0 & \varepsilon'_{II} \end{bmatrix}$$

Case II

$$\underline{\underline{\varepsilon}} = \begin{bmatrix} \varepsilon_{II} & 0 & 0 \\ 0 & \varepsilon_\perp & 0 \\ 0 & 0 & \varepsilon'_\perp \end{bmatrix}$$

Case III

$$\underline{\underline{\varepsilon}} = \begin{bmatrix} \varepsilon_\perp & 0 & 0 \\ 0 & \varepsilon_{II} & 0 \\ 0 & 0 & \varepsilon'_\perp \end{bmatrix} \qquad \text{(iv)}$$

One finds from $\nabla \cdot \vec{D} = 0$ that $A_I = (k_x \varepsilon_\perp / k_z \varepsilon_{II})$ $A_{II} = (k_x \varepsilon_{II} / k_z \varepsilon_\perp)$ and $A_{III} = (k_x / k_z)$ for the three cases respectively. Energy conservation (the wave equation) can be used to relate k_x and k_z for each medium. The boundary conditions for E-tangential and D-normal at the two interfaces can be written as a matrix equation:

$$FC = G \qquad \text{(v)}$$

where

$$C = \begin{bmatrix} \xi_{2p} \\ \xi_{1g} \\ \xi_{2g} \\ \xi_{1a} \end{bmatrix}, \quad G = \begin{bmatrix} -\xi_{1p} \\ -(\varepsilon_p / k_{pz}) \xi_{1p} \\ 0 \\ 0 \end{bmatrix}$$

and

$$F = \begin{bmatrix} 1 & -1 & -1 & 0 \\ -\varepsilon_p/k_{pz} & -\varepsilon_g/k_{gz} & \varepsilon_g/k_{gz} & 0 \\ 0 & F_{32} & F_{33} & F_{34} \\ 0 & F_{42} & F_{43} & F_{44} \end{bmatrix}$$

$$F_{32} = \exp[i\ k_{gz}d],$$

$$F_{33} = \exp[-i\ k_{gz}d],$$

$$F_{34} = -\exp[i\ k_{az}d],$$

$$F_{42} = (\varepsilon_g/k_{gz})\exp[i\ k_{gz}d],$$

$$F_{43} = (-\varepsilon_g/k_{gz})\exp[-i\ k_{gz}d],$$

$$F_{44} = (-A'/k_x)\exp[i\ k_{az}d]$$

A' is determined from the D-normal boundary condition and is given by $A'_I = \varepsilon_{\parallel}A_I$, $A'_{II} = \varepsilon_{\perp}A_{II}$ and $A'_{III} = \varepsilon_{\perp}A_{III}$ for the three cases, respectively.

It is straightforward to find the ratio $r = \xi_{2p}/\xi_{1p}$ and from this the ATR reflectivity, $R = r^*r$.

The wave equation for the anisotropic absorber is[15]

$$-(\omega/c)^2\ \vec{D} = \vec{k}(\vec{k}\cdot\vec{E}) - k^2\vec{E} \qquad \text{(vi)}$$

The equation can be used to obtain k_{az} from k_x. For the three cases considered here:

$$k_{az}^2 = (\omega/c)^2\varepsilon_{\perp} - k_x^2(\varepsilon_{\perp}/\varepsilon_{\parallel}) \quad \text{(Case I)} \qquad \text{(vii)}$$

$$k_{az}^2 = (\omega/c)^2\varepsilon_{\parallel} - k_x^2(\varepsilon_{\parallel}/\varepsilon_{\perp}) \quad \text{(Case II)} \qquad \text{(viii)}$$

$$k_{az}^2 = (\omega/c)^2 \varepsilon_{\perp} - k_x^2 \qquad \text{(Case III).} \qquad \text{(ix)}$$

This concludes the derivation of the ATR reflectivity for anisotropic materials with special orientations.

FIGURE CAPTIONS

Fig. 1. Special orientation geometry and dispersion relations. OA is the optic axis direction and k is the SEW propagation direction for each case. The dispersion relations are also listed along with the general condition for SEW to exist. The additional conditions are found in the text.

Fig. 2. The real part of the dielectric functions of MnF_2. The subscripts $\parallel$ and $\perp$ refer to the diagonal tensor components relative to the optic axis.

Fig. 3. Dispersion curves for MnF_2. The solid line is Case I, the dash-dot line is Case II and the dashed line is Case III. The arrows A indicate the terminating points of the extraordinary SEW. The Case I and Case III curves are overlapping for the second branch on the scale. The line labeled "light line" is the free space photon dispersion line and the line labeled "silicon line" is the maximum momentum available with a silicon ATR prism.

Fig. 4. The ATR reflectance surface of Case I MnF_2. The reflectance is plotted in the vertical direction as a function of the frequency, ω, and the incident angle, θ. The gap spacing is 2.0 μm. The frequency range is 100 cm^{-1} to 500 cm^{-1} and the incident angle is 20°-80°.

Fig. 5. The ATR reflectance surface of Case II MnF_2. The gap spacing is 2.0 μm. ω varies from 100 cm^{-1} to 500 cm^{-1} and θ from 20° to 80°.

Fig. 6. The ATR reflectance surface of Case III MnF_2. The gap spacing is 2.0 μm. ω varies from 100 cm^{-1} to 500 cm^{-1} and θ from 20°-80°.

Fig. 7. The ATR reflectance surface for Case I MnF_2. The gap spacing is 0.5 μm. ω varies from 100 cm^{-1} to 500 cm^{-1} and θ varies from 20°-80°.

Fig. 8. Fixed angle cross sections of the reflectance surface of Fig. 7. The curves are offset for clarity; one division on the ordinate is a change of 10% in reflectance. The angles are indicated. Note that the first minimum terminates while the second remains.

Fig. 9. Experimental ATR spectra of Case I MnF_2. The incident angle is fixed at 30°. The division along the ordinate are reflectance increments of 10%.

Fig. 10. Experimental dispersion curves for Case I and Case III. The solid line is the Case I dispersion curve and the dashed line is the Case III dispersion curve (see Fig. 3). The triangles are the experimental data points for the Case I configuration and the squares are the data points for the Case III configuration. Point A is the theoretical termination point of the Case I extraordinary SEW.

Fig. 11. Experimental ATR spectra showing a terminating branch. The orientation was Case I and the incident angles are as indicated. The gap was approximately 0.5 μm. The curves are offset for clarity. Note the abrupt disappearance of the lower frequency minimum while the minimum at 258 cm^{-1} remains in the spectra at 60°.

Fig. 12. Experimental ATR spectra for Case III. The spectra were obtained at the angles indicated. The curves are offset for clarity; each division on the ordinate is a 10% change in reflectivity. Note that the minimum at 180 cm^{-1} is not present at small angles.

Fig. 13. Fixed angle cross section of the reflectance surface of Fig. 5. This is the Case II orientation with a gap of 2.0 μm. The incident angle is 30°. The small dip at 280 cm^{-1} is the lowest frequency SEW predicted using the dispersion relation.

Fig. A1. ATR Geometry. The incident light is I_o and the reflected light I. The incident angle θ is measured inside the prism and is larger than the critical angle. The gap spacing is d.

REFERENCES

† Work supported by the Air Force Office of Scientific Research under Grant No. AFOSR-74-2654.

1. R.W. Alexander, G.S. Kovener, and R.J. Bell, Phys. Rev. Lett. 32, 154 (1974).
2. G.S. Kovener, R.W. Alexander, Jr., I.L. Tyler, and R.J. Bell, to be published.
3. V.N. Lyubimov and D.G. Sannikov, Sov. Phys. Sol. State 14, 575 (1972) and V.N. Lyubimov, Sov. Phys. Cryst. 17, 714 (1973).
4. K.W. Chiu and J.J. Quinn, Nuovo Cimento 10B, 1 (1972).
5. E.D. Palik, R. Kaplan, R.W. Gammon, H. Kaplan, J.J. Quinn, and R.F. Wallis, Physics Letters 45A, 143 (1973).
6. J.J. Brion, R.F. Wallis, A. Hartstein, and E. Burstein, Phys. Rev. Lett. 28, 1455 (1972).
7. I.L. Tyler, B. Fischer, and R.J. Bell, Opt. Comm. 8, 145 (1973).
8. A. Otto, Z. Physik 216, 398 (1968).
9. V.V. Bryksin, D.N. Mirlin, and I.I. Reshina, JETP Lett. 16, 315 (1972).
10. V.V. Bryksin, D.N. Mirlin, and I.I. Reshina, Sov. Phys. Sol. State 15, 760 (1973).
11. H.J. Falge and A. Otto, Phys. Stat. Sol. (b) 56, 523 (1973).

12. C.H. Perry, B. Fischer, and W. Buckel, Solid State Comm. 13, 1261 (1973).

13. A. Hartstein, E. Burstein, J.J. Brion and R.F. Wallis, Surf. Sci. 34, 81 (1973).

14. J.H. Weaver, C.A. Ward, G.S. Kovener and R.W. Alexander, Submitted to J. Chem. Phys. Solids.

15. A. Sommerfeld, Optics: Lectures on Theoretical Physics Vo. IV, (Academic, New York 1964).

TABLE I. MnF_2 Oscillator Model Dielectric Function Parameters[14]

$\varepsilon_\perp$			$\varepsilon_\parallel$		
ω_{tj} (cm^{-1})	$\delta\varepsilon_j$	γ_j	ω_{tj} (cm^{-1})	$\delta\varepsilon_j$	γ_j
160.0	3.774	0.0283	279.0	1.460	0.0129
251.4	0.224	0.0780	283.8	2.202	0.0389
354.4	1.534	0.0725	369.6	0.224	0.7333
$\varepsilon_\infty = 1.92$			$\varepsilon_\infty = 2.01$		

I

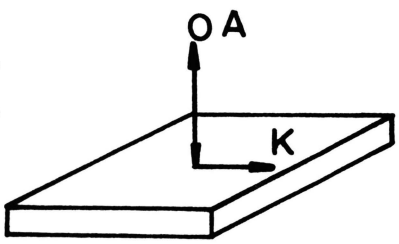

$$k = \frac{\omega}{c}\sqrt{\frac{\epsilon_{\parallel}\epsilon_{\perp} - \epsilon_{\parallel}}{\epsilon_{\parallel}\epsilon_{\perp} - 1}}$$

$$\epsilon_{\perp} < 0$$

II

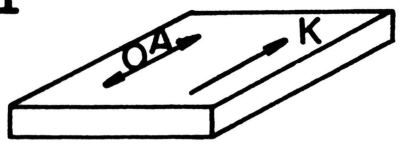

$$k = \frac{\omega}{c}\sqrt{\frac{\epsilon_{\parallel}\epsilon_{\perp} - \epsilon_{\perp}}{\epsilon_{\parallel}\epsilon_{\perp} - 1}}$$

$$\epsilon_{\parallel} < 0$$

III

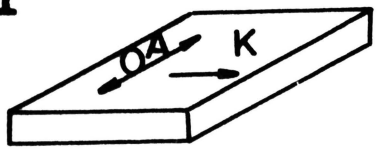

$$k = \frac{\omega}{c}\sqrt{\frac{\epsilon_{\perp}}{\epsilon_{\perp} + 1}}$$

$$\epsilon_{\perp} < -1$$

Figure 1.

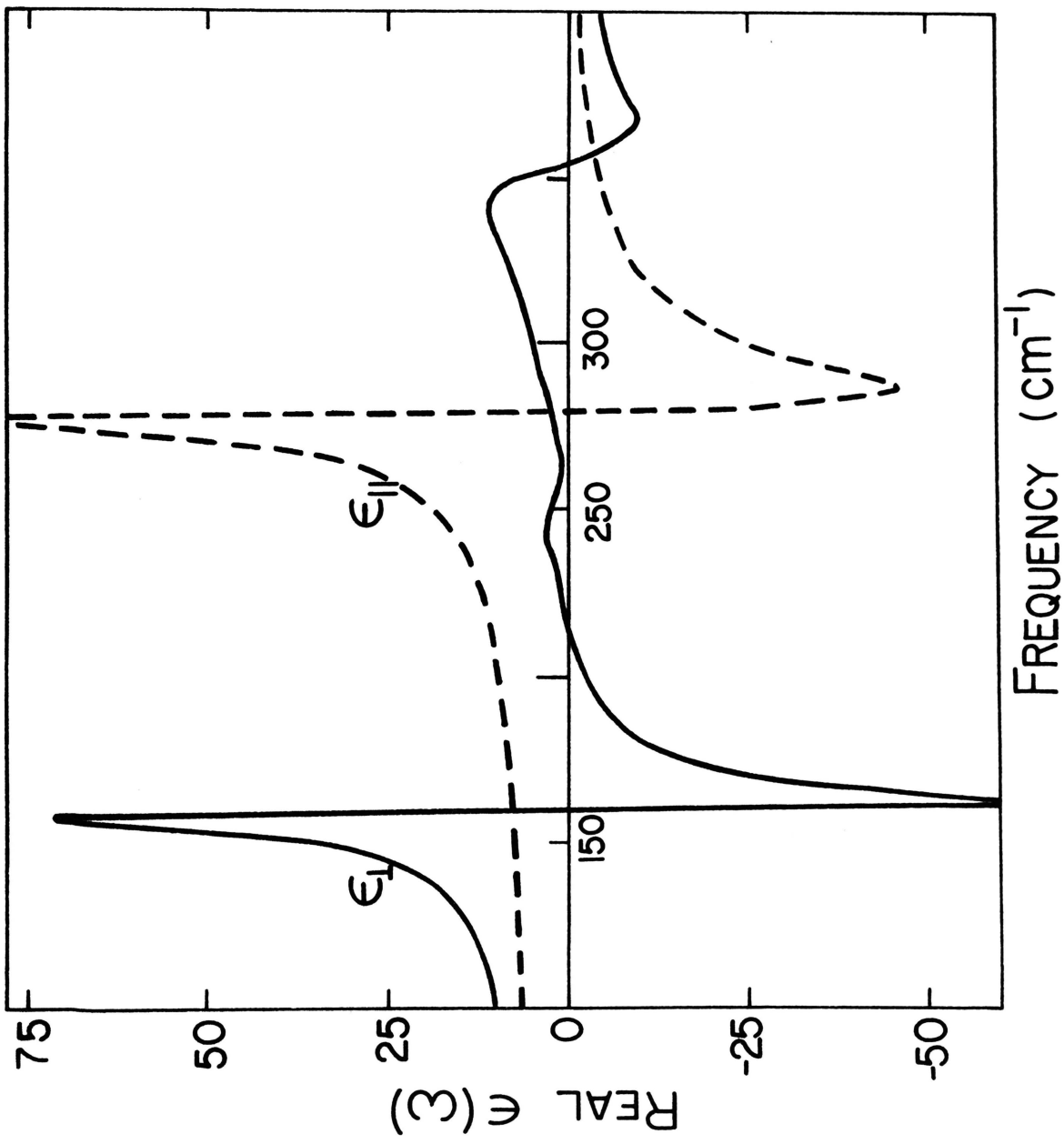

Figure 2.

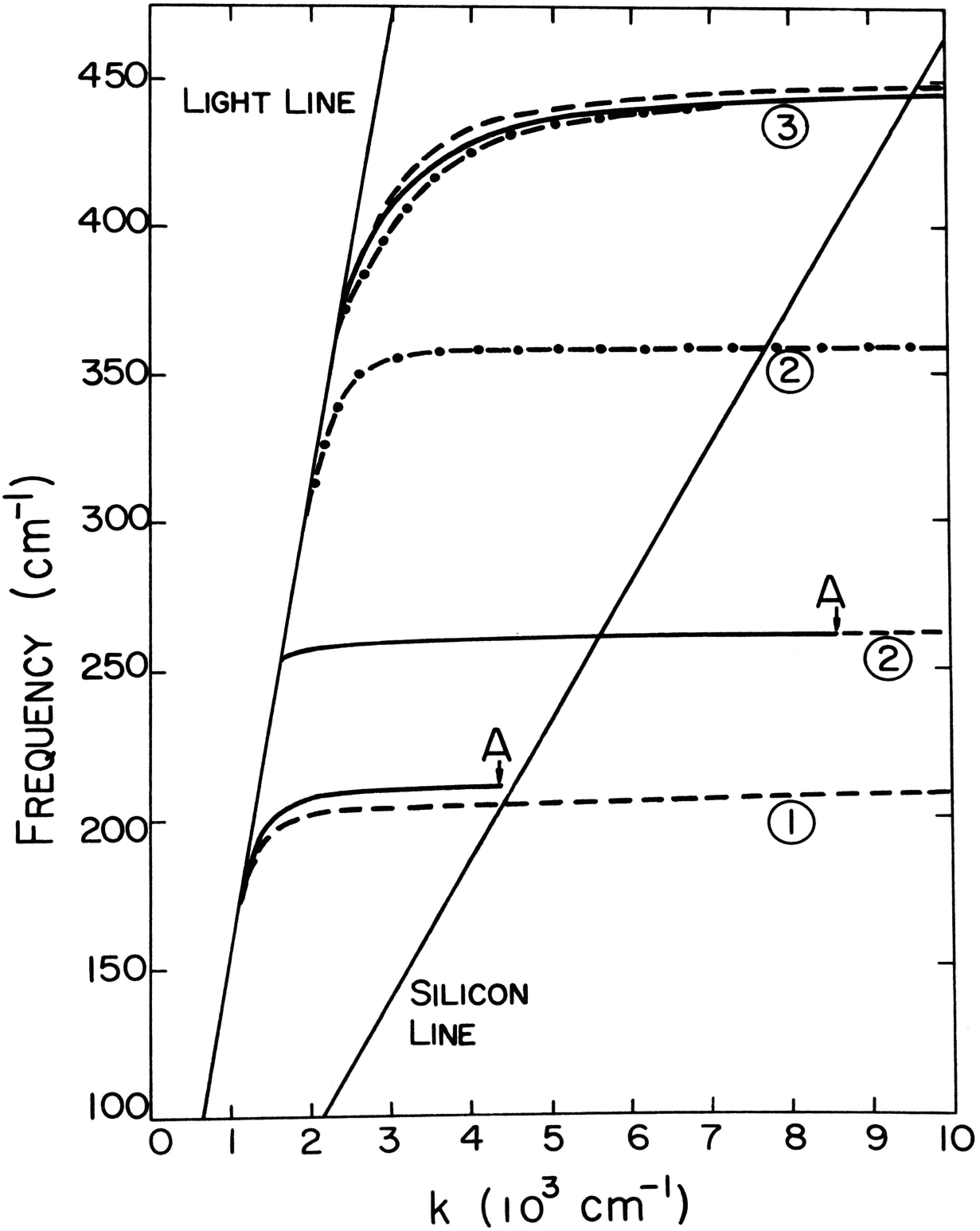
LIGHT LINE
SILICON LINE
A
A
3
2
2
1
FREQUENCY (cm⁻¹)
k (10³ cm⁻¹)
450
400
350
300
250
200
150
100
0
1
2
3
4
5
6
7
8
9
10

Figure 3.

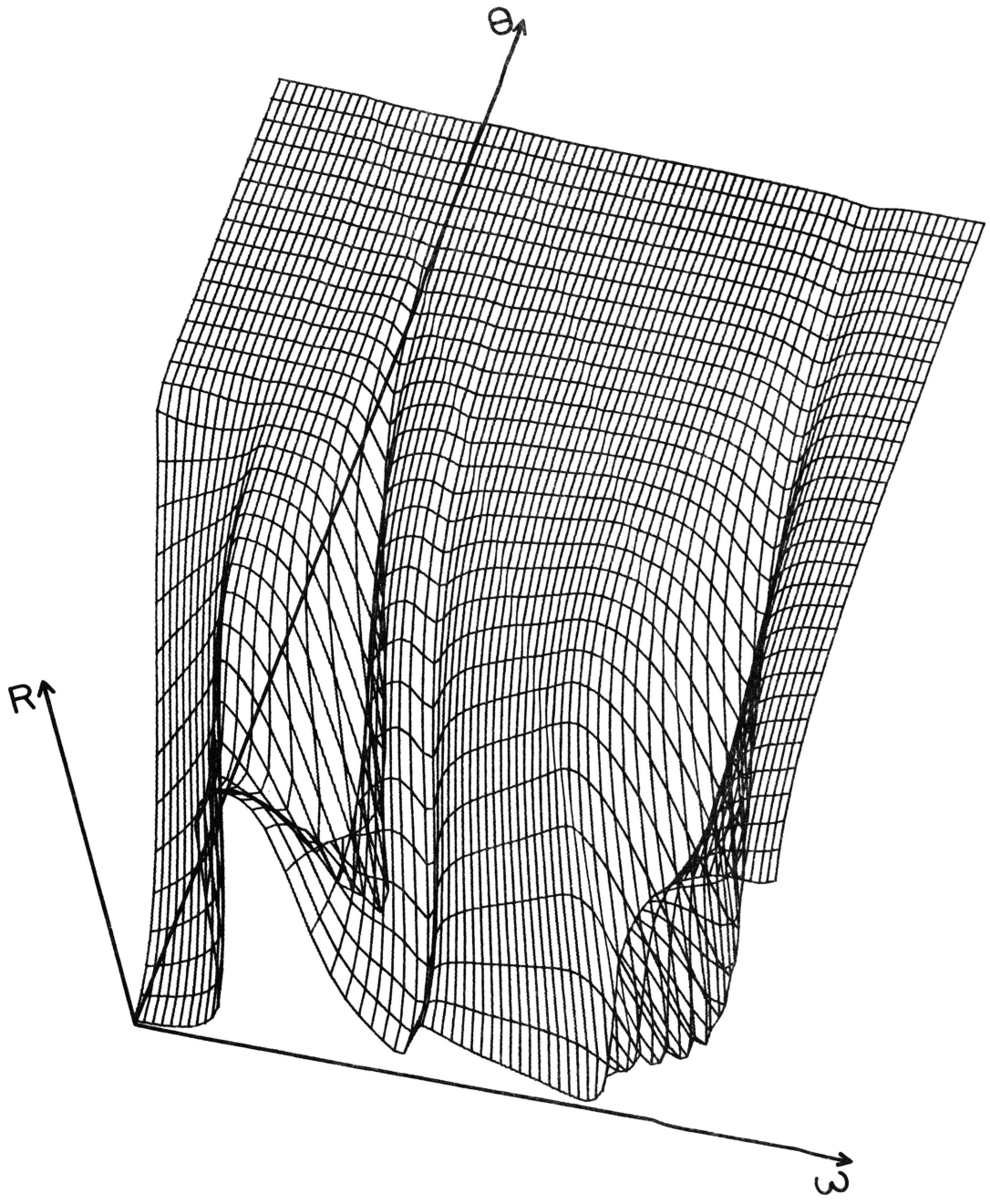

Figure 4.

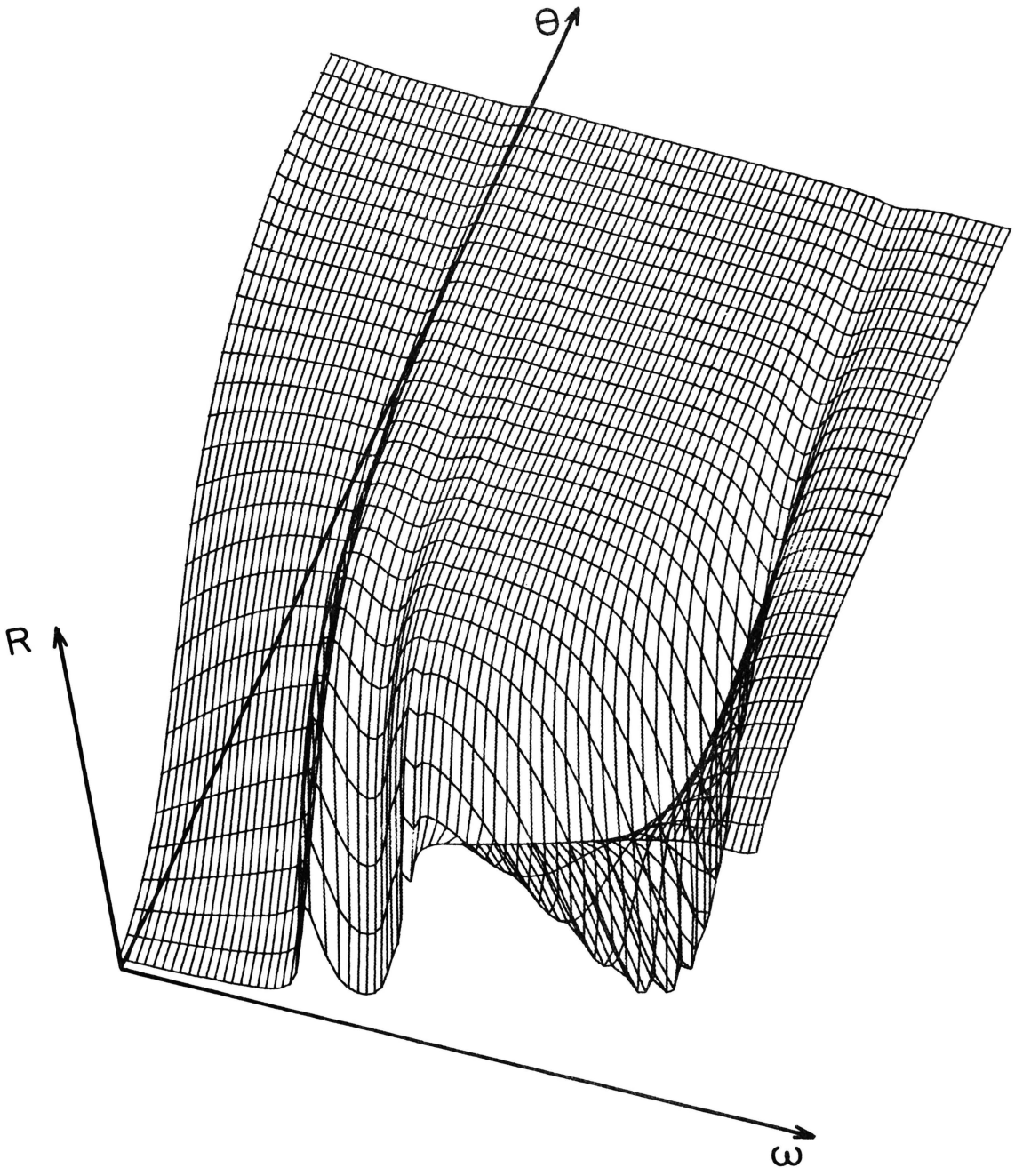

Figure 5.

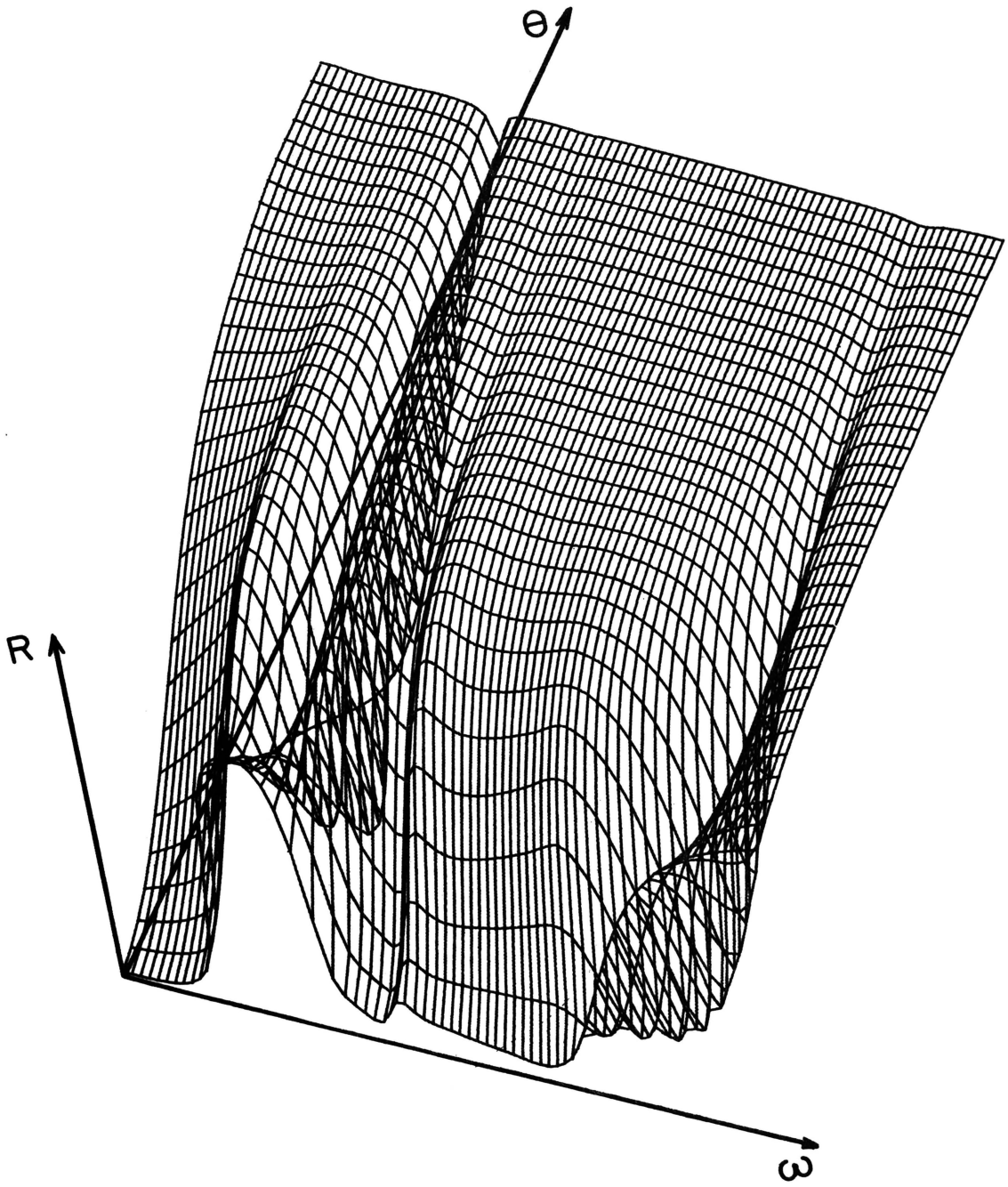

Figure 6.

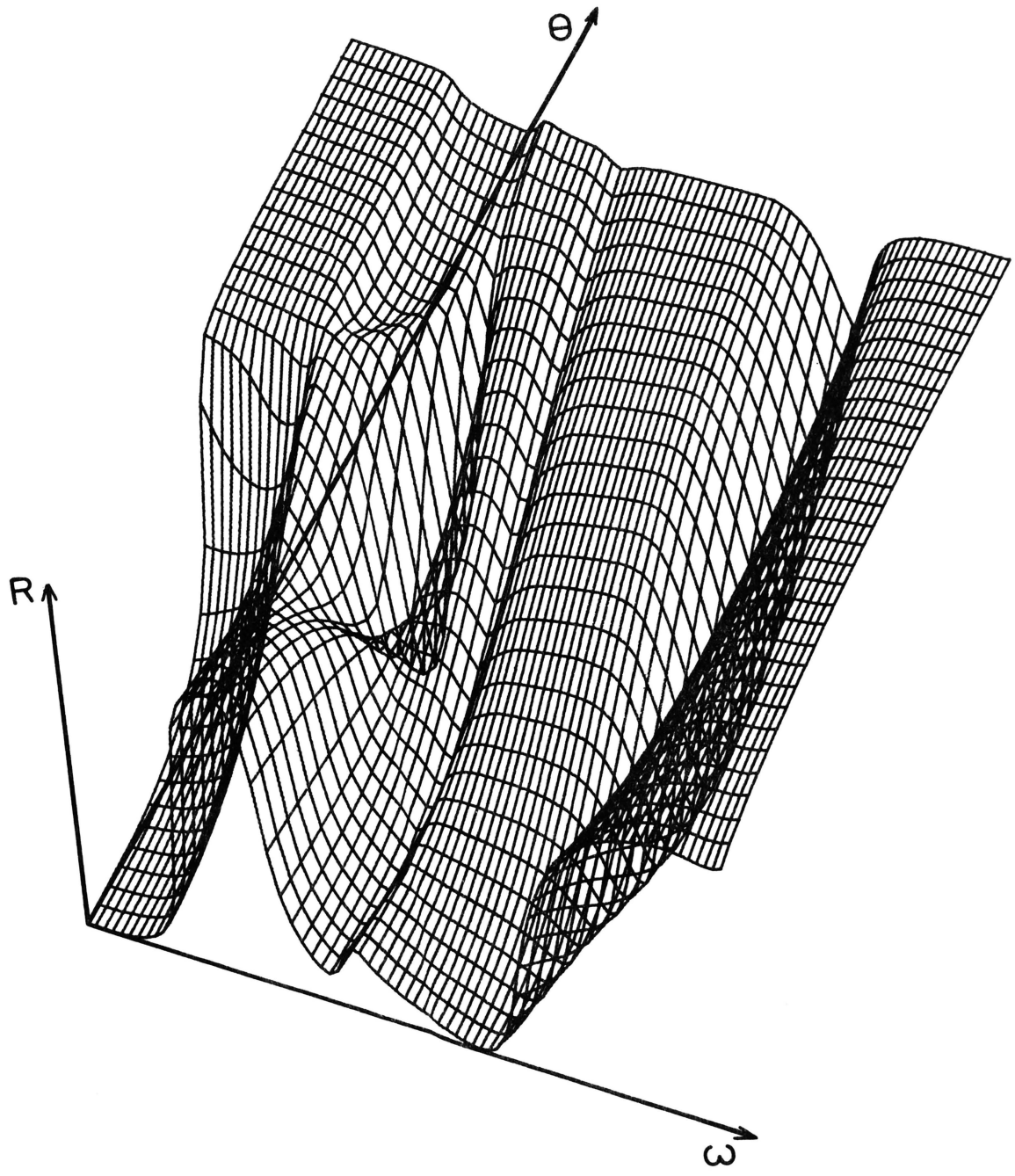

Figure 7.

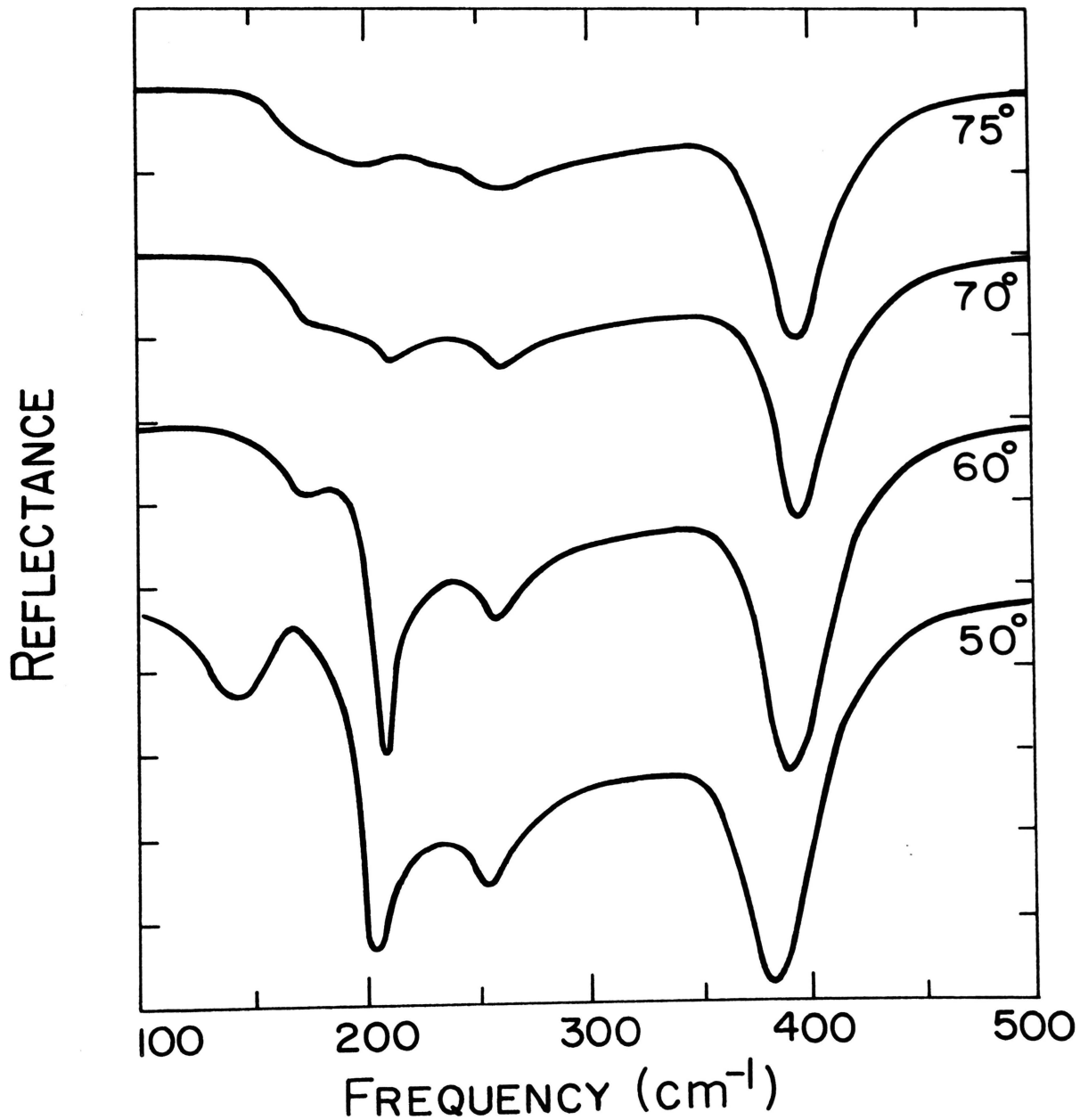

Figure 8.

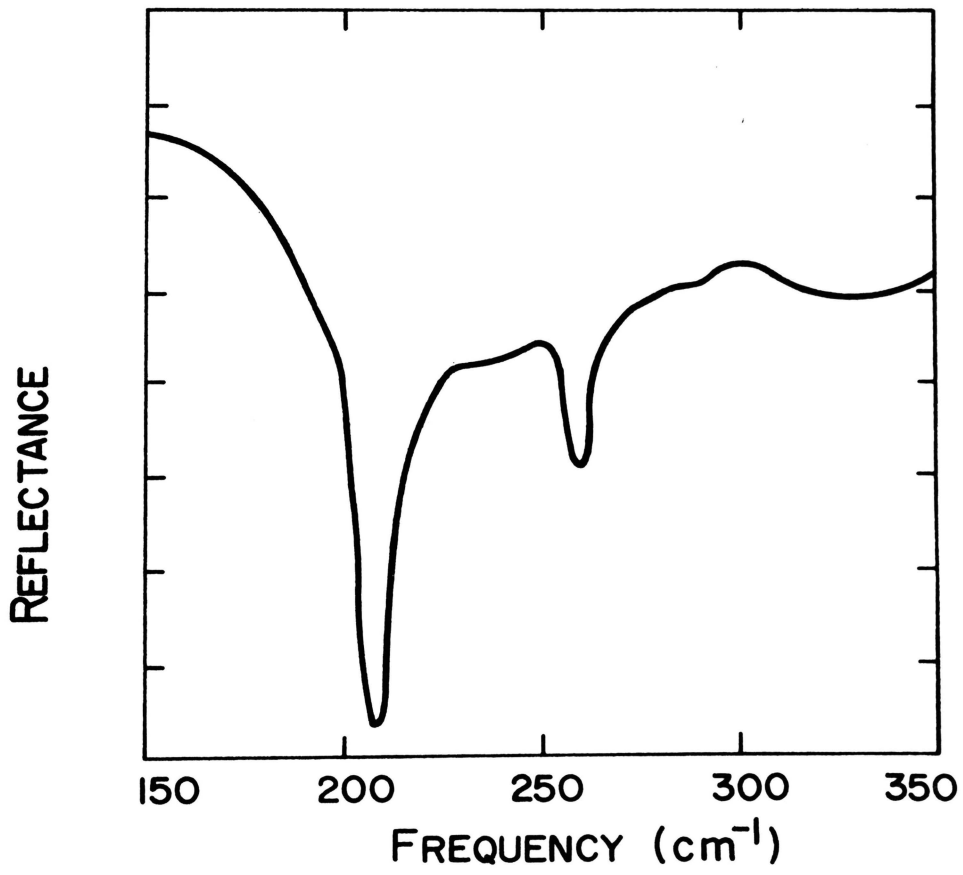

Figure 9.

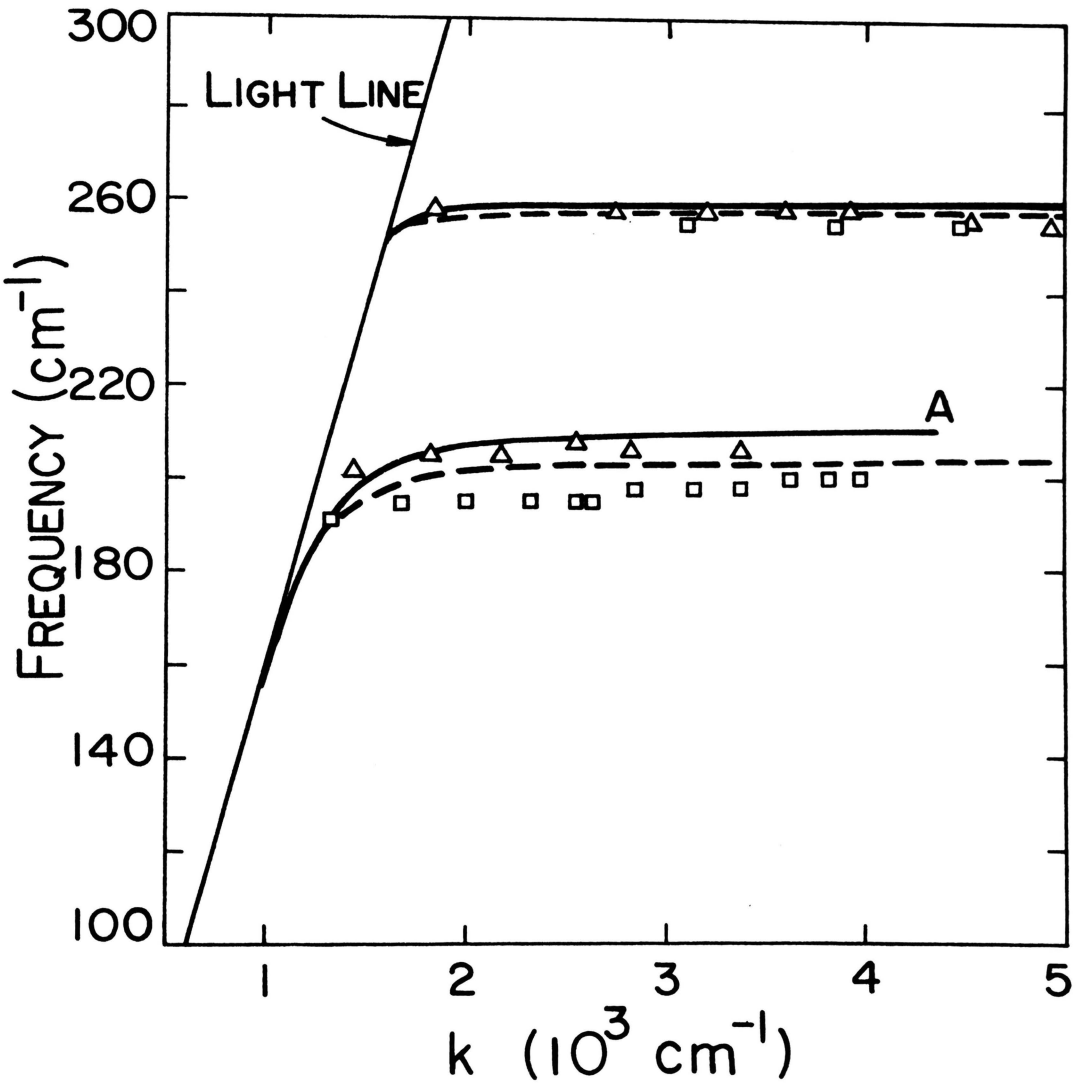
300
260
220
180
140
100
FREQUENCY (cm⁻¹)
LIGHT LINE
A
1
2
3
4
5
k (10³ cm⁻¹)

Figure 10.

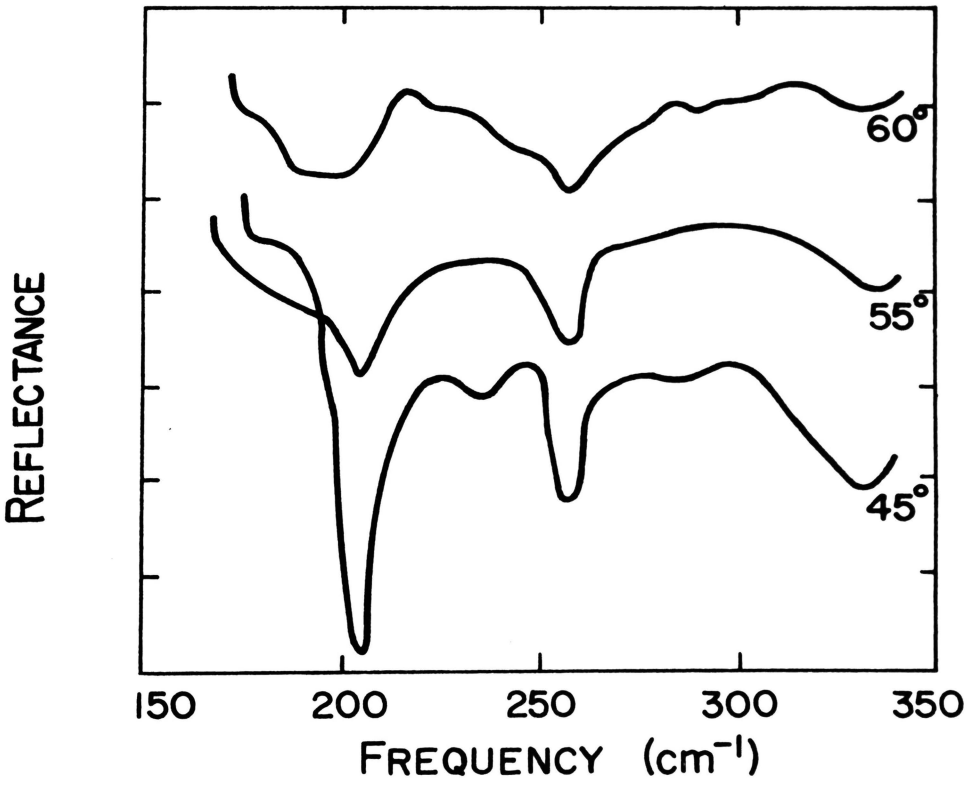

Figure 11.

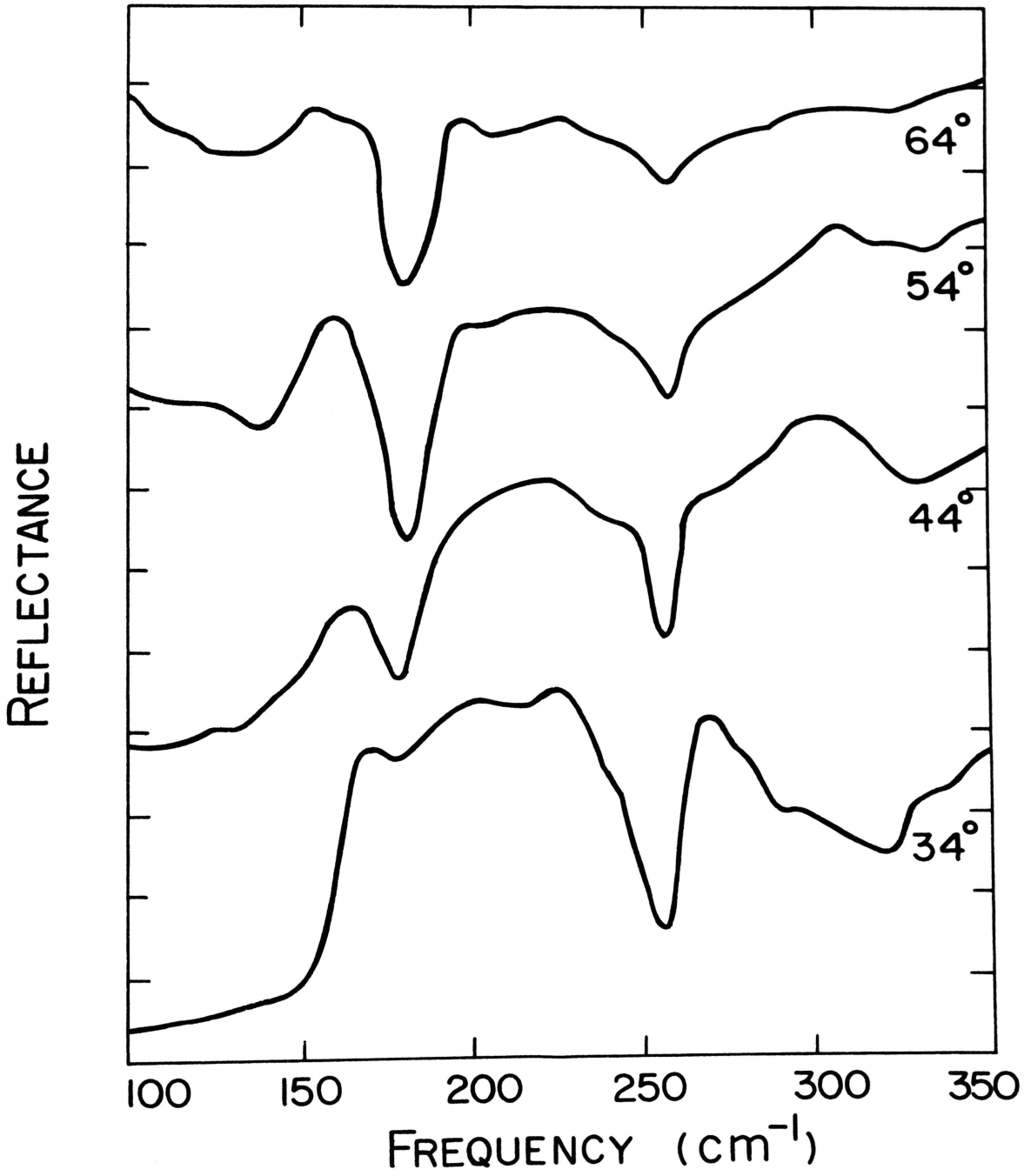

Figure 12.

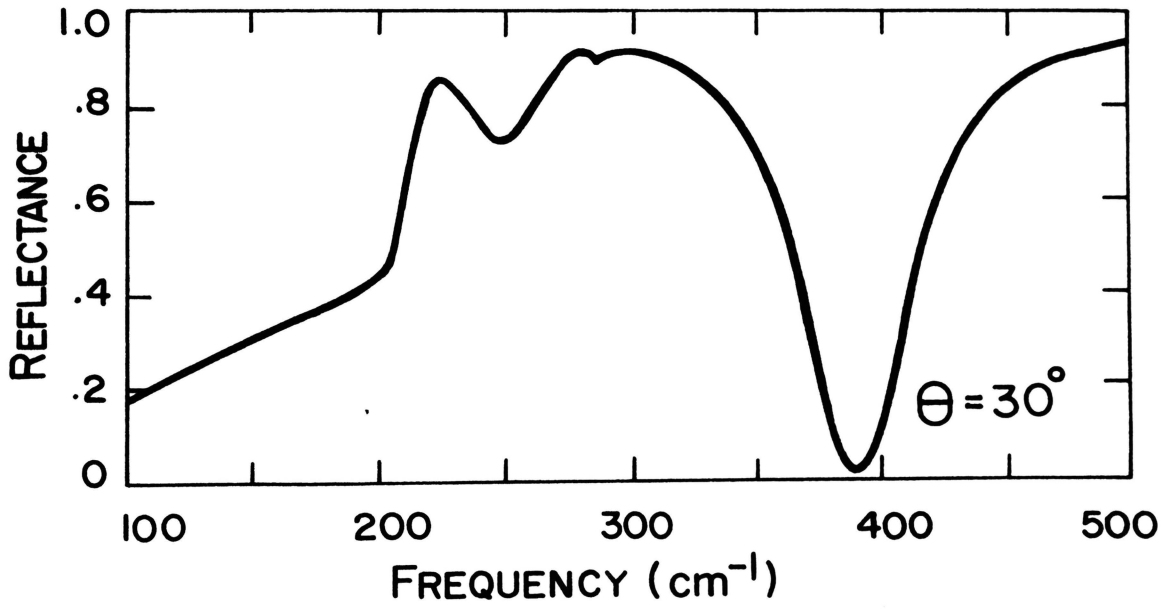

Figure 13.

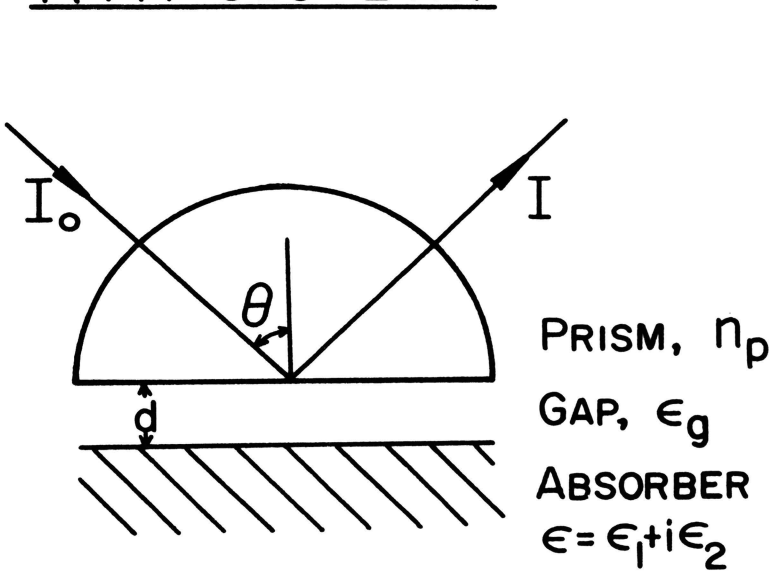
ATR GEOMETRY
I_o
I
θ
d
PRISM, n_p
GAP, ϵ_g
ABSORBER
$\epsilon = \epsilon_1 + i\epsilon_2$

Figure A1.

ACKNOWLEDGEMENTS

We would like to thank Dr. J.H. Weaver for his aid in collecting the experimental reflectivity data and Ms. C.A. Ward for her programming help and significant contribution to the Appendix derivation. The assistance of Mr. L. Teng and Mr. G. Sharp in equipment construction is appreciated. Our discussion with Dr. A. Otto was also very helpful.

VITA

Gary Shannon Kovener was born on September 13, 1946 in Seymour, Indiana. He received his primary and secondary education in Seymour. He has received a Bachelor of Science (with Honors) degree in physics from Indiana University in 1968 and a Master of Science degree in physics from the University of Illinois in 1970.

While working on his Doctorate of Philosophy, he was a teaching assistant and a research assistant with support from THEMIS, National Science Foundation, Air Force Office of Scientific Research, and the Graduate Center for Materials Research--Space Sciences Research Center.